# Title: Carotid Wall Longitudinal Motion in Ultrasound Imaging

## Subtitle: An expert consensus review

## Authors:

Fereshteh Yousefi Rizi (1)
Jason Au (2)
Heikki Yli-Ollila (3), (4)
Spyretta Golemati (5)
Monika Makūnaitė (6)
Maciej Orkisz (7)
Nassir Navab (8), (9)
Maureen MacDonald (10)
Tiina Marja Laitinen (4)
Hamid Behnam (11)
Zhifan Gao (12)
Aimilia Gastounioti (13)
Rytis Jurkonis (6)
Didier Vray (14)
Tomi Laitinen (4)
André Sérusclat (15)
Konstantina S. Nikita (16)
Guillaume Zahnd (8)

(1) School of Electrical and Computer Engineering, College of Engineering, University of Tehran, Tehran, Iran
(2) Schlegel Research Institute for Aging, University of Waterloo, Waterloo, Canada
(3) Department of Radiology, Kanta-Häme Central Hospital, Hämeenlinna, Finland
(4) Department of Clinical Physiology and Nuclear Medicine, Kuopio University Hospital, Kuopio, Finland
(5) Medical School, National and Kapodistrian University of Athens, Greece
(6) Biomedical Engineering Institute, Kaunas University of Technology, Kaunas, Lithuania
(7) Univ Lyon, Université Claude Bernard Lyon 1, INSA-Lyon, UJM-Saint Etienne, CNRS, Inserm, CREATIS UMR 5220, U1206, 7 avenue Jean Capelle, 69621 Villeurbanne cedex, France
(8) Computer Aided Medical Procedures, Technische Universität München, Boltzmannstraße 3, 85748 Garching bei München, Germany
(9) Computer Aided Medical Procedures, Johns Hopkins University, Baltimore, MD, USA
(10) Department of Kinesiology, McMaster University, Hamilton, Canada
(11) Biomedical Engineering Department, School of Electrical Engineering, Iran University of Science and Technology (IUST), Tehran, Iran
(12) School of Biomedical Engineering, Sun Yat-sen University, China
(13) Department of Radiology, Perelman School of Medicine, University of Pennsylvania, USA
(14) Univ Lyon, INSA-Lyon, Université Claude Bernard Lyon 1, UJM-Saint Etienne, CNRS, Inserm, CREATIS UMR 5220, U1206, 7 avenue Jean Capelle, 69621 Villeurbanne cedex, France
(15) Department of Radiology, Louis Pradel Hospital; Hospices Civils de Lyon; Université Lyon 1, Lyon, France
(16) Biomedical Simulations and Imaging Laboratory, School of Electrical and Computer Engineering, National Technical University of Athens, Greece

**Corresponding author:**
Fereshteh Yousefi Rizi
Control and Intelligent Processing Center of Excellence, School of Electrical and Computer Engineering, College of Engineering, University of Tehran, P.O. Box 14395-515, Tehran, Iran.
E-mail: yousefi.f@gmail.com

# Title: Carotid Wall Longitudinal Motion in Ultrasound Imaging

## Subtitle: An expert consensus review

**Abstract:** Motion extracted from the carotid artery wall provides unique information for vascular health evaluation. Carotid artery longitudinal wall motion corresponds to the multiphasic arterial wall excursion in the direction parallel to blood flow during the cardiac cycle. While this motion phenomenon has been well characterized, there is a general lack of awareness regarding its implications for vascular health assessment or even basic vascular physiology. In the last decade, novel estimation strategies and clinical investigations have greatly advanced our understanding of the bi-axial behavior of the carotid artery, necessitating an up-to-date review to summarize and classify the published literature in collaboration with technical and clinical experts in the field. Within this review, the state-of-the art methodologies for carotid wall motion estimation are described, and the observed relationships between longitudinal-motion-derived indices and vascular health are reported. The vast number of studies describing the longitudinal motion pattern in plaque-free arteries, with its putative application to cardiovascular disease prediction, point to the need for characterizing the added value and applicability of longitudinal motion beyond established biomarkers. To this aim, the main purpose of this review is to provide a strong base of theoretical knowledge, together with a curated set of practical guidelines and recommendations for longitudinal motion estimation in patients, to foster future discoveries in the field, toward the integration of longitudinal motion in basic science as well as clinical practice.

**Keywords:** Carotid Artery; Ultrasound; Longitudinal Motion; Cardiovascular Risk Factors; Vascular Health; Atherosclerosis; Arteriosclerosis; Motion Estimation; Speckle-Tracking; Block-Matching

# Introduction

The carotid artery is often referred to as the "sentinel of atherosclerosis", this vessel being a common site of early-stage development of the disease (Rusconi, et al. 2011). The presence and progression of pathological manifestations of systemic vascular disease can be monitored with a myriad of medical imaging modalities. Ultrasound is relatively inexpensive, time-efficient, non-invasive and non-ionizing, (trans-) portable, and offers a spatial resolution that is well suited for the study of large vessels such as the carotid artery. One of the most important aspects of ultrasound is its capacity to achieve temporal imaging, thus enabling the acquisition of cine loops (i.e., movies composed of image sequences) at a frame rate of 30 Hz or more. Such an asset makes possible the analysis of wall distension and associated dynamic metrics of arterial stiffness and strain, which are known pre-clinical markers of cardiovascular disease (CVD) in both healthy and clinically diseased populations (Townsend, et al. 2015). For all these reasons, carotid ultrasound exams for CVD screening are widely integrated in routine clinical practice worldwide.

The motion of arterial tissues during the cardiac cycle is relevant within the context of CVD risk evaluation, as mechanical deformation reflects vessel elasticity, and is putatively inversely associated with arterial stiffness, an independent predictor of all-cause mortality and morbidity (Ben-Shlomo, et al. 2014). Importantly, the degree of disease burden in preclinical or subclinical stages can be evaluated in the carotid artery by quantifying the alteration of the biomechanical tissue dynamics, specifically the shear, stretch, and compression of the vessel wall (Mozaffarian, et al. 2015) (Vlachopoulos, et al. 2011). During the cardiac cycle, the multi-layered carotid artery wall follows a repeatable and complex pulsatile behavior. Different well-established motion types include cross-sectional distension (Gamble, et al. 1994) and circumferential strain (Swillens, et al. 2011). Of recent interest is the so-called "*longitudinal motion*", corresponding to the displacement

of the tissue layers in the direction parallel to the blood flow, namely, along the long axis of the vessel (Persson, et al. 2003) (Figure 1).

The study of longitudinal wall motion has seen an increasing amount of interest over the last two decades, with more recent studies unveiling a complex motion pattern, and suggesting that measures of longitudinal wall motion may offer distinct and independent information for CVD risk prediction and vascular health compared to established risk factors (Svedlund, et al. 2011) (Zahnd, et al. 2012) (Taivainen, et al. 2018). An extensive description of the pathophysiology of arteriosclerosis and atherosclerosis relevant to longitudinal motion is available in the Supplementary Material. While significant strides have been made in the measurement and interpretation of carotid artery longitudinal motion, it has been ignored by most vascular investigations, contributing to a relative paucity of knowledge, while the regulatory mechanisms and implications of longitudinal motion on the vascular system remain to be fully determined. Ultimately, the actual added value of longitudinal motion in comparison to the use of traditional biomarkers for CVD risk detection still needs to be determined.

To comprehensively describe longitudinal motion and its implications, experts in the field have been solicited to contribute to this consortium review, within the scope of plaque-free carotid wall in preclinical and subclinical arteries. Readers interested in plaque-motion assessment may refer to the Supplementary Material. The two main objectives of this project are: 1) review the methodological developments in the quantification of longitudinal wall motion in humans; and 2) review the evidence examining the relationships between longitudinal wall motion and risk factors, independent of conventional markers of radial and circumferential stiffness. To this end, this paper is structured to cover the state-of-the-art methodological and clinical achievements in the field, targeting both scientific and clinical audiences.

# Carotid artery longitudinal motion

## Seminal observations

Longitudinal motion was first observed by studying the motion of markers placed on the surface of the open abdominal aortic artery in dogs (Lawton and Greene 1956). Although this initial study demonstrated a distinct motion along the axis of the vessel, the measured amplitude was relatively small, and the phenomenon was attributed to breathing-induced motion. These findings have then been reproduced by other teams in the thoracic artery of dogs (Patel, et al. 1969) (Patel, et al. 1961) and rats (Deng, et al. 1994). Due to the coarse resolution of ultrasound scanners along the lateral direction at the time, longitudinal motion was often neglected as the cross-circumferential motion was more prominent (Nichols, et al. 1997). Nevertheless, a study involving the tracking of piezoelectric element markers sutured onto the porcine carotid artery (Tozzi, et al. 2001) confirmed the existence of longitudinal motion, independent of breathing-related causes and with an amplitude approximately equal to half of the inner-diameter variation. Subsequently, the presence of a well-defined motion pattern with a magnitude of approximately one millimeter (similar to the amplitude of the motion across the radial direction) was verified *in vivo* in the carotid artery in humans (Persson, et al. 2003) (Golemati, et al. 2003) using B-mode ultrasound images. A growing interest then developed in the scientific and clinical communities, and a number of studies were carried out to progressively characterize this phenomenon, as described in the remainder of this section. Longitudinal motion is often referred to with a slightly different terminology between various research groups of the community, as for example “Longitudinal Kinetics” (LOKI (Zahnd, et al. 2015a)) or “Carotid Artery Longitudinal Wall Motion” (CALM (Au, et al. 2017)). The generic term “longitudinal motion” will be adopted throughout the present article.

## Initial thorough characterization

The first thorough characterization of longitudinal motion was performed by Cinthio *et al*. in 2006 (Cinthio, et al. 2006). Motion of the vessel tissues during the cardiac cycle was precisely measured with a so-called "*echo tracking*" method (Cinthio, et al. 2005) in the common carotid arteries of ten healthy subjects. Several crucial findings were established and corroborated by subsequent studies, as described below.

### Presence of a multiphasic pattern

Longitudinal motion obeys a specific motion pattern with four distinct phases during the cardiac cycle, as displayed in Figure 1. A primary anterograde motion in early systole, in the same direction as the blood flow (also called the A1 phase, or systolic anterograde phase), a retrograde motion, later in systole (R phase, or systolic retrograde phase), a secondary anterograde motion, in diastole (A2 phase, or diastolic anterograde phase), and a gradual return to the equilibrium position. The immediate reproducibility of the phenomenon was also validated via the acquisition of ultrasound clips for a duration that ranged between four and six consecutive cardiac cycles, which has been replicated in subsequent investigations (Ahlgren, et al. 2012) (Au, et al. 2018b) (Cinthio, et al. 2018).

### Presence of an intramural shear stress and shear strain

Longitudinal motion was assessed within regions at different depths within the wall layers (namely, intima-media complex, tunica adventitia, and surrounding tissues). It was observed that the overall motion amplitude was decreasing with intramural depth, thus generating a longitudinal shear stress and shear strain within the tissues (Cinthio, et al. 2006). Comparing simultaneous measurements between the intima-media and adventitial regions, reproducible assessment of the inter-layer strain angle could be performed, which corresponded approximately to one radian. A

variety of phenomena related to longitudinal shear were assessed in subsequent studies, and the corresponding findings are reported in the dedicated subsection "Characterization based on intramural shear strain and shear stress".

Presence of longitudinal motion in peripheral arteries

It was further investigated whether longitudinal motion was present in other arteries (Cinthio, et al. 2006). Measurements were conducted in a subset of three healthy volunteers, in the abdominal aorta, the brachial artery, and the popliteal artery. Although the phenomenon was less marked, the presence of longitudinal motion and the accompanying intramural shear strain was confirmed in these peripheral arteries. The discrepancy in amplitude was putatively due to several factors, such as the physiological differences in the arterial tree, the muscular nature of both the abdominal and brachial arteries, the deeper location of the aorta causing a lower frame-rate, the smaller motion resulting in noisier measurements, and the greater distance to the heart. The vast majority of the studies published since have thus been focusing on the carotid artery, as the small displacements of the peripheral arteries have not been demonstrated to be as reproducible as in the central vasculature. The remainder of this review specifically refers to carotid artery longitudinal motion.

# Methodological approaches

Since the initial evaluation of carotid wall longitudinal motion in humans *in vivo* (Persson, et al. 2003) (Golemati, et al. 2003), an increasing number of motion-tracking techniques have been designed to address this task (Golemati, et al. 2012) (Golemati, et al. 2016). Several challenges inherent to either ultrasound imaging (e.g., speckle noise and artifacts) or vessel physiological behavior (e.g., abrupt motion patterns) must be considered for reliable motion-tracking. As a result,

specialized and advanced methodologies were gradually developed to specifically extract longitudinal motion.

## Wall motion extraction based on B-mode images

B-mode is the most well-known representation of ultrasound imaging: this modality, characterized by a specific grayscale speckle pattern, is used to represent structural information that can be interpreted visually on the scanner monitor. Three major motion-tracking approaches are used to extract the motion from B-mode ultrasound image sequences: block matching (BM), optical flow (OF), and feature matching (FM). These techniques, and the related studies focusing on longitudinal motion, are listed in Table 1 and discussed thereafter. Further approaches based on computer-aided diagnosis were also introduced, mostly to investigate the severity of atheromatous plaques, and are discussed in the Supplementary Material.

### Block matching

Block matching is a conventional technique in the field of motion estimation, and widely used to perform speckle tracking in image sequences. The general underlying principle is to find, within the $(n+1)^{st}$ image, the most probable location of a target region, denoted as the reference pattern, from the $n^{th}$ image. Estimation is performed either by minimizing a difference metric with operators such as the sum of squared differences, or by maximizing a similarity metric with operators such as the normalized cross correlation. Among the most critical parameters is the size of the analyzed speckle pattern and of the maximal authorized displacement (namely, the "block" and the "search window", respectively).

Strategies directly based on traditional BM have been successfully applied to assess longitudinal motion. In an early study (Golemati, et al. 2003), the extracted motion waveforms were rather coarse, likely due to a large block size and no sub-pixel interpolation. However, thus obtained

158 reproducible and well-defined patterns contributed to the feasibility of *in vivo* examinations. A
159 BM method known as "echo tracking", using a small block size (originally defined as a 0.7×0.7
160 $mm^2$ region), enabled accurate tracking of salient speckles in carefully acquired images (Cinthio,
161 et al. 2005). Nevertheless, reduced block sizes are unlikely to provide robust results in general
162 routine clinical scans, where image quality is often poor.

163 Adaptive BM approaches were introduced to tackle the issue of speckle decorrelation across time.
164 Such approaches generally correspond to a mathematical model involving a control scheme, as
165 well as an evolution scheme, capable of representing the expected temporal motion and
166 compensating for tracking errors. The Kalman filter was exploited to model the temporal changes
167 in the location of the target block (Gastounioti, et al. 2011) (Gastounioti, et al. 2013), as well as in
168 its gray levels (Gastounioti, et al. 2011) (Gastounioti, et al. 2013) (Zahnd, et al. 2013) during the
169 cardiac cycle.

170 A BM approach based on the consideration of two previous frames (as opposed to only one in the
171 classical techniques) was proposed to increase the tracking robustness (Albinsson, et al. 2014).
172 Adding one extra reference block in a BM scheme was proposed to use different reference blocks
173 (Albinsson, et al. 2014): here, the actual pixel values of the previous frame were used, as opposed
174 to Kalman-based methods, where the reference block was predicted. A more advanced method
175 was later proposed, involving an affine block motion model, able to consider rotation and scaling
176 of the tracked pattern, in addition to rigid translation (Golemati, et al. 2012). A scheme based on
177 luminance optimization was also proposed to take into consideration the progressive variations of
178 pixel values across time and to maximize the matching potential (Yli-Ollila, et al. 2013).

179 A nonlinear state-space approach based on an elasticity model of the carotid wall and including a
180 $H_\infty$ filter was further proposed and adapted to carotid wall motion estimation (Gao, et al. 2016)
181 (Gao, et al. 2017b) (Gao, et al. 2017a). The major benefit of these approaches is their ability to

deal with noisier data and provide robust and accurate tracking results when conventional BM approach would likely fail.

The combined use of multiple blocks was investigated in several studies. These approaches are based on the following principle: at a given time-step, the motion is independently estimated with a series of adjacent or partly overlapping blocks, and the resulting motion is obtained via the averaging of all contributions. The rationale for multi-block matching is to increase the robustness by diminishing the influence of any single block that may fail. Such approaches include five (Zahnd, et al. 2011b), six (Tat, et al. 2017), or sixteen (Zahnd, et al. 2012) blocks. A method based on the consideration of multiple frames per estimation and a parabolic sub-sample interpolation in high frame-rate cine loops (1300–1500 Hz) was further developed (Albinsson, et al. 2018). Several advanced search strategies, initially introduced in radiofrequency imaging (Shi and Varghese 2007) (Lopata, et al. 2009), were successfully applied in B-mode imaging to improve computation time, such as a coarse-to-fine interpolation scheme (Zahnd, et al. 2011b) and a sparse-to-dense tracking scheme (Albinsson, et al. 2014).

Going one step further, the extraction of a dense motion field was recently addressed (Zahnd, et al. 2018). Here, the temporal motion across the full width of the image is estimated by placing a block in each column (typically, more than 350). A combinatorial analysis scheme based on dynamic programming is used to simultaneously extract the motion of each block (as opposed to one after the other), while enforcing motion rules and enabling fast computational times. Results from this study enabled assessing the degree of motion homogeneity across the length of the vessel.

Optical flow

Optical flow consists in determining the velocity field across different temporal frames (Horn and Schunck 1981). The fundamental difference between OF and BM is the adoption of the Eulerian paradigm (i.e., motion is evaluated through a static window) instead of the Lagrangian scheme

(i.e., motion is evaluated by dynamically following a target). Complex motions involving rotations and deformations are usually better captured via OF-based approaches than BM (Hein and O'brien 1993).

Applied in the context of carotid longitudinal motion, OF has been successfully used in several studies (Murray, et al. 2007) (Golemati, et al. 2012) (Salles, et al. 2012), as listed in Table 1. It was shown that the general waveform shape of the wall motion was different when extracted by BM and OF, although their peaks occurred at the same time instants of the ECG signal (Stoitsis, et al. 2006). The maximum velocity and extracted motion in the radial and longitudinal direction was shown to be greater using BM (Stoitsis, et al. 2006). The estimated wall motion on the same B-mode images by OF and BM in radial direction were reported to be more similar compared to the longitudinal direction (Stoitsis, et al. 2006). In the presence of either Gaussian or speckle noise, it has been reported that weighted least-squares OF outperformed BM, particularly in poor-quality images that are typically observed in clinical populations (Golemati, et al. 2012).

Feature matching

An original approach based on automatic extraction of several salient image regions was recently introduced (Scaramuzzino, et al. 2017). Detectors such as Scale-Invariant Feature Transform (SIFT), Speed Up Robust Features (SURF), and Maximally Stable Extremal Regions (MSER) were used to identify target points. The main advantage of this approach is its robustness, since only salient points are considered for tracking, and re-selected at each time-step. Moreover, this method has potential to be fully automatic since regions are determined by the above-mentioned descriptors. Additionally, shear strain evaluation in different anatomical layers is also possible by using feature matching via the tracking of points located in different anatomical layers, offering a similar potential for depth-specific shear evaluation as provided by certain BM approaches (Shi, et al. 2008) (Idzenga, et al. 2014). However, a generally encountered drawback of FM approaches

is the constant re-selection of target points and the averaging of their respective motion vectors, making both precise single-point and full dense-field motion estimation impossible.

**Wall motion extraction based on radiofrequency signals**

Tracking methodologies based on radiofrequency (RF) signals were introduced in 1985 to estimate the radial motion via an autocorrelation approach (Kasai, et al. 1985). As opposed to B-mode imaging, RF-based motion tracking involves the computation of the phase shift (i.e., in the frequency domain) between two subsequent time steps to determine the corresponding spatial displacement. Of note, acquisition and export of RF signals usually necessitates research-oriented scanners, as this functionality is generally not available in clinical devices. An overview of the approaches developed toward carotid wall motion estimation is summarized in Table 2, and detailed thereafter.

Concerning small inter-frame displacements, a BM-based method has been developed in an iterative manner (Albinsson, et al. 2018). Phase-based estimation on radio-frequency signals has been applied on phantom and in vivo carotid for simultaneous wall motion and flow estimation (Hasegawa and Kanai 2008b) (Perrot, et al. 2017) (Perrot, et al. 2018a) (Fekkes, et al. 2018). Phase-sensitive methods have been recently applied for 2D motion estimation using 2D frequency spectra of RF echo signals using the complex analytical signal obtained by modulating the ultrasonic field (Jensen and Munk 1998), by the Hilbert transform (Chen, et al. 2004) (Sumi 2008) (Hasegawa and Kanai 2009) (Salles, et al. 2015), or by the wavelet transform (Rizi, et al. 2014) (Yousefi Rizi, et al. 2014). The Hilbert transform was repeatedly used to generate a complex analytical signal from RF data using correlation-based estimators (Hasegawa and Kanai 2009). Following a similar approach, phase correlation and sub-sample interpolation were successfully applied (Zambacevičienė and Jurkonis 2019). Fourier-based methods (Hasegawa and Kanai 2006a) (Hasegawa and Kanai 2006b) (Hasegawa and Kanai 2008a) were also introduced. A paired

1D and 2D motion estimation technique with shifted cross spectra developed to assess the phase shift was put forward, and showed increased accuracy with a smaller spatial window than conventional 2D motion estimators (Hasegawa 2016). One advantage of Fourier-based approaches is their intrinsic ability to achieve sub-pixel accuracy without the need for spatial interpolation, which can result in greater accuracy compared to speckle tracking in B-mode (Miyajo and Hasegawa 2018) (Miyajo, et al. 2019). It was shown that the 2D phase-sensitive method (Miyajo and Hasegawa 2018) outperformed BM method in terms of accuracy (bias errors and standard deviations) in motion estimation at a high frame rate that was realized by parallel beamforming (Miyajo, et al. 2019). This is especially important along the longitudinal direction of the artery, since the image across this axis is generally coarser than the radial counterpart.

An approach relying on synthetic aperture imaging was specifically designed as an unconventional beamforming strategy to generate a pressure field with a controlled carrier frequency in the transverse direction (Jensen and Munk 1998). This real-time technique, referred to as "US-tagging" (in reference to the principle of magnetic resonance imaging tagging), consists of the transmission of an unfocused wave, subsequently received with a dynamic quadratic focusing combined to dynamic apodization (Chen, et al. 2004) (Liebgott, et al. 2007). Building upon the potential offered by such marked signals, a local phase-based optical flow method was devised for subpixel estimation (Basarab, et al. 2009), and was applied in vivo in the context of longitudinal motion on so-called RF-2D images (Zahnd, et al. 2015b). A similar approach leveraging high frame-rate imaging (10,000 Hz) was also introduced (Salles, et al. 2015), bridging the gap between the association of longitudinal motion and pulse wave velocity (PWV). For 2D velocity vector estimation of tissue motion, plane wave imaging has been used along with transverse oscillation and an efficient frequency domain estimator (Salles, et al. 2015). It is noteworthy that unitary displacements greater than half of the signal wavelength (be it determined by the carrier frequency along the radial direction, or by the synthetic aperture along the longitudinal direction) cannot be

ascertained via phase-tracking methods, since they fall under the effect of aliasing (Basarab, et al. 2009) (Hasegawa 2016), therefore justifying the demand for a sufficiently high frame-rate.

Inspired by the field of computer vision, an approach known as "motion video amplification" was proposed to magnify the tiny and subtle deformation of the vessel wall in B-mode ultrasound carotid image sequences (Perrot, et al. 2018b). While large-scale deformations are not amplified, low-amplitude deformations within the vessel wall (such as longitudinal motion, radial motion, deformation caused by the passage of the pulse wave) are substantially magnified up to a factor of 1000, and can be easily perceived by a clinician with the naked eye. This technique opens up new possibilities for the evaluation of complex motion patterns, as the small phase W and phase X displacements described in Section "Characterization based on directional wall displacements". Of note, this technique requires the acquisition of high frame-rate sequences (>2500 Hz), which is only available on a limited number of research-oriented ultrasound systems.

**Available tools**

The Velocity Vector Imaging (VVI) software platform (VVI, Research Arena 2; TomTec Imaging Systems GmbH, Unterschleissheim, Germany) is a commercially available tool that was used to investigate the association of longitudinal motion with cardiovascular risk in man and mouse (Svedlund, et al. 2011) (Svedlund and Gan 2011a) (Svedlund and Gan 2011b). This technique, initially designed to measure heart dynamics, involves the positioning of a multi-segment horseshoe-shaped skeleton in the image, using a total of 20 control points. Applied to the carotid artery, one segment (approximately 5 mm long) can be positioned on a region of interest in the intima-media complex. Of note, the VVI displays the measured temporal trajectory, together with the corresponding motion amplitude, but does not support any export of the time series for finer analysis. Despite relevant clinical findings (Svedlund, et al. 2011) (Svedlund and Gan 2011a) (Svedlund and Gan 2011b), a thorough evaluation of the tracking performances (Zahnd, et al.

2013) demonstrated poor accuracy and reproducibility, while being tedious and time consuming due to substantially high amount of manual operations required to run VVI.

The MyLab desktop analysis software (Esaote, Firenze, Italy) is a commercially available tool that was used to extract longitudinal shear values (Zhang, et al. 2014). However, although this technique was specifically designed for ultrasound carotid data, quantitative reports of the tracking performance per se are not publicly available, to the best of the authors' knowledge.

The CAROLAB software platform (Zahnd, et al. 2019) is a freely available[1] tool that has been put forward to analyze ultrasound image sequences of the carotid artery. The motivation behind CAROLAB is to encapsulate several previously published and thoroughly validated methodologies for wall segmentation (Zahnd, et al. 2017b) and motion estimation (Zahnd, et al. 2013) (Zahnd, et al. 2018) within an efficient graphical user interface.

A web-based platform named CAROTID has been developed, integrating motion-based Computer-Aided Diagnosis (CAD) functionalities for patients with carotid atherosclerosis (Gastounioti, et al. 2014).

# Clinical studies

A growing body of work has contributed to establish a number of associations between carotid wall longitudinal motion and vascular health. Although all findings are based on longitudinal motion analysis, different types of motion-derived features have been considered, and the literature on plaque-free wall motion can be classified in the following three main categories. First, the total amplitude of the wall excursion, also referred to as the peak-to-peak amplitude, has been used to quantify the overall wall displacement. Second, the intramural shear strain has been evaluated by

[1] https://www.creatis.insa-lyon.fr/carolab/

measuring the motion across the depth of the different tissue layers. Third, the directional wall displacements based on the tri-phasic waveform, corresponding to the specific and complex shape and pattern of the trajectory, has been studied to characterize the different anterograde and retrograde phases during the cardiac cycle. Additional studies specifically involving the motion of atheromatous plaques are mentioned in the Supplementary Material.

**Characterization based on peak-to-peak motion amplitude**

Peak-to-peak motion amplitude has been repeatedly demonstrated to bear an association with cardiovascular health status, while being independent from established cardiovascular risk factors and other noninvasive measures of arterial stiffness and subclinical carotid atherosclerosis (Svedlund, et al. 2011) (Zahnd, et al. 2012) (Taivainen, et al. 2017). Although peak-to-peak amplitude does not capture the tri-phasic complexity of the full motion pattern, it is an easily described measurement that provides general information about longitudinal wall motion. A number of findings, detailed hereafter, indicate that longitudinal motion does not simply replicate information already captured by other indices and markers, but instead represents added value to CVD risk estimation.

Peak-to-peak motion amplitude was observed to vary with age in an inverted-U shaped relationship (Cinthio, et al. 2018) (Au, et al. 2019), as well as to demonstrate a progressive decline in magnitude as a function of disease status. In comparison to younger adults, longitudinal motion amplitude was significantly reduced in elderly patients with coronary artery disease (n=16; 0.54 *vs*. 0.11 mm (Svedlund and Gan 2011b)), in elderly diabetic patients (n=26; 0.48 *vs*. 0.31 mm (Zahnd, et al. 2011b)), as well as in adults with periodontal disease (n=126: 0.42 *vs*. 0.15 mm (Zahnd, et al. 2012)). Moreover, the peak-to-peak amplitude of longitudinal motion was found to be decreased with the presence of coronary artery disease or myocardial ischemia, independent of arterial stiffness (n=14 (Au, et al. 2017)). The effects of catecholamine and beta-blockade was

investigated, demonstrating profound changes in longitudinal displacement and intramural shear strain of the porcine carotid artery (n=5 (Ahlgren, et al. 2011)) (n=5 (Ahlgren, et al. 2009)). An inverse correlation was shown between systolic blood pressure and both the peak-to-peak amplitude and the retrograde motion amplitude (n=19 (Yli-Ollila, et al. 2013)) (n=287 (Taivainen, et al. 2018)). The association between longitudinal motion and conventional measures of arteriosclerosis was further supported, with the peak-to-peak and retrograde amplitudes being directly correlated with carotid artery distensibility and inversely correlated with PWV, independent of brachial flow-mediated dilatation and intima-media thickness (IMT) (n=292 (Taivainen, et al. 2017)). It was also demonstrated that the peak-to-peak motion amplitude represented a predictor for 1-year cardiovascular outcome in patients with suspected coronary artery disease, independent of cross-sectional stiffness and IMT (n=441 (Svedlund, et al. 2011)). A study conducted in a children population established a weak correlation between longitudinal motion and arterial stiffness, indicating that longitudinal motion is not a reliable surrogate marker of arterial stiffness in children (n=191 (Proudfoot, et al. 2019)). In a multi-ethnic study, a notable but non-statistically significant association was found to support that longitudinal displacement predicted coronary heart disease and cardiovascular disease events (n=389 (Gepner, et al. 2015)) and (n=791 (Gepner, et al. 2019)). Comparing the peak-to-peak amplitude in wall regions located closer to the head or closer to the heart, it was reported that the measured amplitude was consistently reduced in sites further away from the heart, potentially due to a progressive attenuation of the forces along the length of the artery (Zahnd, et al. 2015a).

**Characterization based on intramural shear strain and shear stress**

Wall shear strain is theorized to play a role in atherosclerosis progression and vasa vasorum circulation (De Korte, et al. 2011). The fundamental impact of longitudinal shear strain and longitudinal shear stress onto vascular health and arterial aging has been shown via theoretical

hemodynamic models (Humphrey, et al. 2009). Shear strain can be calculated based on the amplitude of longitudinal motion of intima-media, adventitia and surrounding tissue at end-diastole and at maximum excursion (Cinthio, et al. 2006). It was found that the amplitude of longitudinal motion was greater when measured in regions of interest (ROIs) located within innermost tissues compared to more peripheral ROIs, which can be explained by the fact that the intima-media complex, with a larger relative elastin component, is more compliant, whereas the collagen-rich adventitia is likely fixed to the surrounding tissues. Shear strain was initially quantified *in vivo* in ten healthy volunteers with angles close to 1 radian (Cinthio, et al. 2006). Similar results were reported by considering the mean maximum shear strain of healthy volunteers (n=10) (Nilsson, et al. 2010). Building upon these findings, another study investigated the presence of intramural shear strain between elderly diabetic patients (n=14), elderly healthy controls (n=14), and young healthy controls (n=14): for both healthy cohorts, a sharp shearing angle, corresponding roughly to 1 radian, was perceptible between the intima-media complex and the tunica adventitia, whereas the shearing pattern was substantially more attenuated for the at-risk cohort, potentially reflecting stiffer vessels (Zahnd, et al. 2011a). The retrograde intramural shear strain, as well as the retrograde amplitude in both the intima-media complex and adventitia layer, were reported to be significantly reduced in individuals with spinal cord injury (n=7) compared to able-bodied controls (n=7) (Tat, et al. 2017). Finally, the presence of a temporal delay between the motion of the different layers was reported in 20 healthy subjects: longitudinal motion was initiated in the intima-media complex, and reached the tunica adventitia after 18.9 ms, on average (Yli-Ollila, et al. 2016b).

**Characterization based on directional wall displacements**

Although the presence of a general multiphasic bidirectional pattern was established (cf. Section "Presence of a multiphasic pattern") (Cinthio, et al. 2006), a certain amount of inter-subject

variability has been repeatedly reported (Ahlgren, et al. 2012) (Yli-Ollila, et al. 2013) (Yli-Ollila, et al. 2016b) (Yli-Ollila, et al. 2016a) (Taivainen, et al. 2017) (Zahnd, et al. 2017a) (Qorchi, et al. 2017) (Cinthio, et al. 2018). Motion patterns were found to be subject-specific, and can either be described as retrograde-oriented, bidirectional, or anterograde-oriented (Ahlgren, et al. 2011) (Yli-Ollila, et al. 2013) (Au, et al. 2018a), as illustrated in Figure 2. However, regardless of inter-subject variability, intra-subject longitudinal waveform patterns have been shown to remain stable over a 4-month period (Ahlgren, et al. 2012), over a 12-month period in children (Au, et al. 2019), as well as in response to 12 weeks of supervised exercise training in healthy adults (Au, et al. 2020). These results suggest that motion waveform patterns contain more information that the bare peak-to-peak amplitude, and may be viewed as "vascular fingerprints" or "vessel signatures", which can putatively represent complementary information toward vascular health evaluation. It is however noteworthy that a certain amount of intra-subject variability was reported, in both beat-to-beat and day-to-day situations (n=10) (Ahlgren, et al. 2012), (n=10) (Au, et al. 2016), (n=19) (Yli-Ollila, et al. 2013): for this reason, it was recommended to analyze the average of four consecutive waveforms (Au, et al. 2018b).

Three general motion patterns observed in a range of healthy adults have been defined (Yli-Ollila, et al. 2013): primarily anterograde (forwards from the equilibrium position), primarily retrograde (backwards from the equilibrium position), and bi-directional (oscillating around the equilibrium position). The three primary phases (i.e., A1, R, A2) of longitudinal motion are thought to be regulated by systemic factors such as local shear stress, blood pressure, and left ventricular rotation (Cinthio, et al. 2006) (Ahlgren, et al. 2015) (Au, et al. 2016) (Yli-Ollila, et al. 2016a) (Yli-Ollila, et al. 2016b) (Taivainen, et al. 2017) (Au, et al. 2018a) (Proudfoot, et al. 2019). Longitudinal motion of the wall adjacent to plaque has been investigated in some studies and was demonstrated to reveal useful information about the status of the regional tissue area. It was shown that the mean amplitude of longitudinal separation of anterior and posterior walls was similar to their radial

separation (n=29) (Golemati, et al. 2003), as observed in a mixed group of healthy (plaque-free, young and elderly) adults, and symptomatic and asymptomatic plaque patients. Both the systolic anterograde and retrograde components of longitudinal motion are reduced during the early arterial stiffening process (n=19) (Yli-Ollila, et al. 2016a). A study conducted in 292 participants demonstrated that anterograde motion increased and retrograde motion decreased with increasing number of cardiovascular risk factors (Taivainen, et al. 2017). The measured retrograde amplitudes showed an inverse correlation with blood pressure, body mass index, total cholesterol, and triglycerides (n=287) (Taivainen, et al. 2018). While some evidence suggests that the A1 phase may be of value (Taivainen, et al. 2018), other studies have not replicated meaningful cross-sectional associations with arterial stiffness or cardiovascular risk factors (Au, et al. 2017) (Proudfoot, et al. 2019). Taken together, these results are in accordance with the observation that the accumulation of cardiovascular risk factors ultimately lead to a shift toward an anterograde-dominant pattern in individuals with overt atherosclerotic disease (Taivainen, et al. 2017) (Yli-Ollila, et al. 2016a) (Yli-Ollila, et al. 2016b).

The radial-axial length was explored to further characterize the association between longitudinal motion and arterial distension. It was demonstrated that the diameter variation accompanying follows a partly linear relationship with longitudinal motion (n=20) (Yli-Ollila, et al. 2016b). A stable phase difference was also established between the blood pressure signal and longitudinal motion, hence suggesting a direct association between longitudinal motion and arterial stiffness (n=20) (Yli-Ollila, et al. 2016b). The radial-axial displacement can be used to analyze the total length of the corresponding hysteresis loops, as displayed in Figure 3, taking into consideration the full 2D displacement of the arterial wall. Radial-axial length has been shown to correlate with arterial stiffness in healthy adults (n=292) (Taivainen, et al. 2017), and be positively associated with longitudinal motion amplitude in children over a one-year period (n=114) (Au, et al. 2019). The elastic properties of the carotid artery were further analyzed with a model coupling axial and

446 radial stress (n=10 healthy adults), suggesting that both displacement directions are coupled from
447 a biomechanical point of view and should be considered collectively (Soleimani, et al. 2016).

448 A recent study contributed to characterize more finely the multiphasic pattern of the wall with the
449 addition of two distinct phases in the A1-R-A2 scheme: phase W, corresponding to a rapid
450 retrograde motion just prior to the time-point of minimum diameter preceding the A1 phase, and
451 an anterograde phase X, corresponding to a small anterograde movement around the time of the
452 dicrotic notch in the distension wave (Cinthio, et al. 2018). These novel phases were found to
453 noticeably differ between middle-aged and older patients compared to younger patients (n=135)
454 (Cinthio, et al. 2018). Although these phases W and X are not systematically observed in all
455 participants due to their small magnitudes, they may provide additional clues as to how
456 longitudinal motion and radial distension are coupled, particularly at periods of rapid pressure
457 changes such as the arrival of the forward pressure wave and the dicrotic notch, as displayed in
458 Figure 2.

459 To characterize the complex motion waveform patterns in detail, several additional features have
460 been proposed, but not yet widely adopted. Peak velocity and acceleration were demonstrated to
461 be relevant parameters associated with cardiovascular risk factors (Yli-Ollila, et al. 2016a) (Yli-
462 Ollila, et al. 2016b). The root mean square value was introduced to quantify the waveform
463 integrated intensity, and could be used to discriminate at-risk participants (n=49) from healthy
464 controls (n=30) (Makūnaitė, et al. 2019). A variety of so-called "kinematic features", such as
465 Kurtosis and skewness, were also put forward as tentative risk markers for atherosclerosis
466 (Gastounioti, et al. 2014). Motion (in-)homogeneity was recently investigated in a study where the
467 entire width of the exploitable wall image was tracked in 62 elderly patients at high cardiovascular
468 risk (Zahnd, et al. 2018). Here, the amplitude-independent index σX was introduced to quantify
469 the motion similarity between adjacent regions along the length of the vessel. A strong correlation

was observed between σX and the presence of coronary artery disease (β-coefficient =0.586, p=0.003).

## Hypotheses about the factors causing longitudinal motion

Despite the light shed by preliminary studies, understanding of the physiological cause of carotid wall longitudinal motion is still far from complete (Au, et al. 2016) (Au, et al. 2018a). The origin of the local anterograde and retrograde peaks of longitudinal motion in the systolic and diastolic phases of heart cycle have been the focus of initial experimental studies (Cinthio, et al. 2006) (Ahlgren, et al. 2012) (Ahlgren, et al. 2015) (Au, et al. 2016) (Au, et al. 2018a) (Dempsey, et al. 2018). A central problem in developing a mechanistic framework for longitudinal motion is the large inter-subject variability in motion patterns. Further differences in longitudinal motion patterns among subjects of the same age and gender have also been remarked (Ahlgren, et al. 2012). Conceivably, any hypothesis about the origin of longitudinal motion in humans must account for this variability and unify individuals who exhibit dominant anterograde or retrograde wall displacements.

While there is a paucity of experimental evidence to support a central motion hypothesis, emphasis has been placed on a "compartment" model, wherein local wall shear stress dictates the anterograde motion component, while some central cardiovascular phenomenon dictates the retrograde motion component (Au, et al. 2016). With respect to the anterograde longitudinal displacement, the energy resulting from the blood friction could putatively provoke longitudinal motion of the innermost wall layers, which in turn also contributes in some extent to drag the outermost wall layers (Yli-Ollila, et al. 2016b). Temporal alignment of the peak anterograde motion and peak local blood velocity was observed (Cinthio, et al. 2006) (Au, et al. 2016), supporting an initial relationship between these factors. However, follow-up experimental pressor

response studies in both human (Au, et al. 2018a) and porcine (Ahlgren, et al. 2011) (Ahlgren, et al. 2015) models were unable to relate the increased magnitude of wall shear stress to changes in the anterograde motion component, possibly due to confounding changes in blood pressure in response to exaggerated pressor reflexes in both cases. There currently exists no evidence of a causal relationship between the forward shear component and the initial anterograde displacement of the arterial wall.

With respect to the retrograde motion component, a key observation from cross-sectional studies is the fact that retrograde displacement is often of greater magnitude than the preceding anterograde displacement in young adults (Au, et al. 2016). Given the mismatch in displacement magnitudes, it was theorized that active cardiovascular events may be key determining factors in the tri-phasic motion patterns (Cinthio, et al. 2006). For example, the apical traction of the aortic valve annulus in late systole (Simonson and Schiller 1989) could contribute to stretch the carotid artery upstream, while a rigid fixation downstream is provided by both the bifurcation and the petrous portion of the temporal bone where the internal carotid enters the skull. This hypothesis is also supported in pigs, showing that the length of a segment of the common carotid artery changes during the cardiac cycle (Tozzi, et al. 2001), as well as using in vivo B-mode image sequences, and showing that longitudinal motion was substantially larger in regions located close to the heart compared to regions close to the head (Zahnd, et al. 2015a). Only two studies to date have investigated the potential role for cardiac involvement in the regulation of longitudinal wall motion. The temporal- and magnitude-based relationships have been detailed between the retrograde component and both longitudinal excursion of the left ventricular base (a surrogate for displacement of the aortic valve) and rotation of the left ventricle using simultaneous capture of carotid and ventricular motion (Au, et al. 2016). While the excursion of the left ventricular base was unrelated to the retrograde component, the left ventricular rotation was identified as a potential correlate of retrograde magnitude. A follow-up experimental study (Au, et al. 2018a) indicated a

weak-to-moderate relationship between left ventricular rotation and retrograde displacement, providing preliminary evidence for the retrograde component of a compartment model. Indirect evidence from right-left comparisons complicates these findings, where no dependence was found between longitudinal motion amplitude and the echoscopic neck side (Svedlund and Gan 2011b). This is noteworthy since the left common carotid artery is directly connected to the aorta, whereas the right common carotid artery is connected to the aorta via the S-shaped brachiocephalic trunk. Therefore, the initial pulling force by the aortic traction (known as the tricuspid annular plane systolic excursion) should hypothetically be further attenuated in the right side and could potentially be reflected by smaller motion amplitude.

Several other hypotheses regarding the potential causes of longitudinal motion have been proposed, albeit without experimental evidence. Anterograde displacement may also be accounted for by the passage of the pulse wave, locally causing the expansion of the internal diameter, and likely also generating a damping mechanism across the axial direction. While no studies have experimentally investigated the second anterograde (A2) displacement, others have posited that a passive elastic component may dictate a retrograde return to an equilibrium position, making it an ideal candidate for stiffness estimation from longitudinal motion data (Au, et al. 2017). Given that the A2 phase also occurs in anterograde-dominant motion traces, it may also be explained by the multiple reflection and re-reflection pulse waves at the interface of regions with different vascular impedance (Nichols, et al. 1997) that is a probable cause of the second anterograde motion.

Finally, an active component from the wall itself cannot be excluded. It is hypothetically possible that the mechanical deformation of the vessel contributes to the inrush/washout cycle in which the nutriments contained in the blood are transported through the layers to nourish peri-adventitial tissues. The development of specific image-based tools and the design of biophysiological studies are required to further investigate the key evolutionary basis for longitudinal motion.

# Guidelines for optimal image acquisition and analysis

Compared to traditional arterial measurements, such as IMT, image acquisition for the purpose of longitudinal motion estimation is more challenging, as it requires collecting a long high-quality image sequence rather than one still frame. There also is a need for standardizing the acquisition and management of these data. This section is devoted to technical and practical recommendations with respect to these needs.

## Challenges related to longitudinal motion

While conventional measures of arterial distension are concerned with the axial (i.e., along the beam axis) resolution, longitudinal measurements are primarily influenced by lateral (i.e., perpendicular to the beam axis) resolution. In general, lateral resolution is determined by the physical arrangement of the piezoelectric elements in the probe head, and is generally coarser than the axial resolution, which depends on the ultrasound wave carrier frequency. Lateral resolution has a major impact on feature extraction techniques, namely block matching, which relies on stable salient patterns within the vascular wall. This is in part because the arterial wall is composed of several concentric layers, and the gray-level of these regions exhibits a homogeneous longitudinal profile along the vessel length, whereas the radial profile respects a well-defined pattern of intensity change caused by the juxtaposition of several anatomical layers. Optimizing the spatial resolution in the lateral direction will improve motion-tracking quality, ultimately leading to more precise measurements of longitudinal motion.

Several intrinsic factors, such as speckle decorrelation, out-of-plane motion, motion artifacts, acoustic shadowing, and false echoes can degrade ultrasound images. The time-variant contrast and intensity of the carotid ultrasound image, caused by the blood flow, also hinder the motion estimation (Yousefi Rizi, et al. 2014). Another issue to consider is the non-rigid nature of the wall

565 motion, where deformable tissues may cause drastic changes in the tracked speckle pattern
566 (Golemati, et al. 2012). High variability of image quality, due to subject-specific vessel geometry
567 and tissue echogenicity should also be taken into consideration. Extraneous factors, such as
568 scanner model, sonographer expertise and habits, and custom analysis programs also contribute to
569 the variability across different studies. A series of recommendations toward a more efficient and
570 uniform procedure has been proposed (Au, et al. 2018b).

571 **Ultrasound parameter settings**

572 The central frequency of the probe should typically be comprised between 6 and 12 MHz for a
573 satisfactory trade-off between image penetration and axial resolution, as recommended by the
574 Mannheim consensus (Touboul 2015). The focal depth should be set to the far wall. The image
575 depth must fully encompass the region of the far wall and include some peri-adventitial tissues in
576 order to provide enough space for the motion-tracking algorithm to operate (typically between 3
577 and 4 cm deep). Images with a depth beyond 4 cm will result in lower performances because of a
578 poorer frame-rate and a coarser pixel size. To reach sufficient accuracy, the spatio-temporal
579 resolution is recommended to be within the range of 25 Hz or higher for the frame rate, and 50 μm
580 or lower for the pixel size. For studies examining the velocity or acceleration of the wall, the
581 required frame rate should be even greater. The persistence of the scanner should be set to zero to
582 avoid inter-frame blurring. Contrast, brightness, and time gain compensation should be correctly
583 configured so that no regions suffer from under- or over-exposure, specifically limiting
584 background noise in the lumen. The intima-media complex must be clearly visible, and the lumen-
585 intima and media-adventitia anatomical interfaces should appear as a pair of clearly perceptible
586 contours. In the case of an arterial site with an atherosclerotic plaque, the luminal interface should
587 appear as a sharp contour, and if possible, the intima-media complex on both sides of the plaque
588 should also exhibit clearly perceptible edges. The tissues, especially within the intima-media

589 complex, should exhibit a grainy speckle texture. If possible, no marking should be present within
590 the imaging location (e.g., ECG signal trace, manual point or line annotations, text indications
591 such as carotid side or patient name), in order to preserve the original pixel greyscale values that
592 are necessary for the motion-tracking algorithm. The far wall of the common carotid artery should
593 be the primary outcome of motion tracking, as a fluid-tissue echo boundary has improved quality
594 for block-matching algorithms. Images should optimally be exported in DICOM format, rather
595 than via a frame-grabber and video conversion, in order to preserve spatio-temporal quality.

596 The spatio-temporal characteristics of the motion, as well as the capacity of an ultrasound system
597 to resolve them, should be briefly discussed. Regarding the spatial resolution, a generic ultrasound
598 pixel size is typically around 50 μm. Since the peak-to-peak distension amplitude of longitudinal
599 motion is roughly 1 mm, the excursion of the tracked point along the longitudinal direction usually
600 corresponds to less than 20 pixels. This coarse degree of quantization should be considered when
601 attempting to study the details of the trajectory waveforms. Improving the temporal resolution may
602 play a role in improving block-matching success and enhance the sensitivity to detect subtle
603 changes in longitudinal motion over time or between populations. For instance, a typical resting
604 heart rate of 80 beats per minute results in a complete motion cycle of approximately 0.75 seconds.
605 Assuming a general ultrasound frame-rate of 30 Hz, one cycle of longitudinal motion corresponds
606 to 23 images. Given that the large systolic longitudinal displacements would occur in the first third
607 of a cardiac cycle, that leaves only 8 frames to quantify the X, A1, R, and W phases, discussed
608 previously in Section “Presence of a multiphasic pattern”, which is likely inadequate to detect
609 subtle changes in motion phases in an individual over time. Studies that report on specific phases
610 of longitudinal motion typically rely on frame-rates around 60-100 Hz, which is considered as the
611 lower end required to detect rapid changes in wall direction during the cardiac cycle (Cinthio, et
612 al. 2018) (Au, et al. 2017).

## Participant preparation

As acquisition considerations for longitudinal motion are largely similar to that of other vascular measurements, it is recommended to follow the general protocol put forth for similar vascular health evaluation, such as pulse wave velocity (Van Bortel, et al. 2012) and flow-mediated dilation (Thijssen, et al. 2010, Alley, et al. 2014). Procedures should take place in a quiet, temperature-controlled room, with a dim light to improve *in situ* image visualization. Prior to the acquisition, participants should avoid moderate-to-vigorous physical activity for 24 hours, refrain from tobacco or marijuana smoking for 12 hours, and avoid eating or drinking fluids besides water for at least 2 hours. Upon arrival, the participant should be given 10-20 min to relax in the supine position in order to ensure resting heart rate and blood pressure during data collection. During the acquisition, participants should be in the supine position, with the neck slightly extended (Touboul, et al. 2012) (Gutierrez and Rundek 2016). Due to the sensitivity of motion-estimation algorithms and the complexity of longitudinal motion patterns, it is paramount to avoid any artifactual motion while images are being acquired in order to ensure that the motion fully corresponds to the natural displacement of the arterial wall. Therefore, it is crucial that the participant remains perfectly still, with the neck muscles completely relaxed. For short measurements (under 10 seconds), breath-hold of the subject is preferable, in order to reduce breathing-related issues in longitudinal motion tracking. The breath-hold should be performed by avoiding the Valsalva effect (i.e., in the middle of a normal breathing routine, without excessive inspiration prior the breath-hold). In addition, the subject should avoid swallowing saliva and refrain from talking during imaging.

## Image acquisition

One challenge that persists in image acquisition is deciding the location in which longitudinal motion should be measured to standardize observations between subjects. The presence of a progressive attenuation of the motion amplitude along the common carotid artery whereby total

displacement is attenuated closer to the bifurcation was demonstrated (Zahnd, et al. 2015a). In the absence of clear advantages of one method over the other, similar placement as the Mannheim consensus (Touboul 2015) is recommended. If possible, the analyzed region should be a flat (non-tilted, non-curved) segment of the common carotid artery on the far wall. Far wall is preferable over near wall since the fluid-to-tissue echo boundary has improved quality for block-matching algorithms. The probe should be placed two cm away from the carotid bifurcation in such a way that the bifurcation appears on one side of the image to landmark placement with repeated measurements. The probe orientation should also be consistently maintained so that the left and right side of the image correspond to the same direction (e.g., caudal or cranial) across different acquisitions. There is currently no indication whether the right or left carotid artery is preferable for standardizing longitudinal motion measurements; consistency should be maintained for repeated measurements intra- and inter-participants.

The probe should be aligned in the longitudinal vessel axis plane so that out-of-plane motion is as low as possible during the entire cardiac cycle. It is the responsibility of the operator to ensure that the probe remains perfectly static during the entire acquisition. As motion-tracking approaches vary, at least approximately two cm length of wall should be available for analyses. In order to account for intra-individual variability in motion-derived indices, it was demonstrated that averaging the values across four cardiac cycles resulted in a reduced variability of thus measured indices (Au, et al. 2018b). Acquisition should ideally be gated with a simultaneous reference ECG signal.

**Image analysis**

It is recommended to assess longitudinal motion on a specific region of the intima-media complex that remains visible through the entire duration of the clip, such as a salient echo (Cinthio, et al. 2005) or a well-perceptible and contrasted speckle pattern (Zahnd, et al. 2013). In addition, it is

important that the analyzed region (i.e., the distance from the carotid bulbus) is kept constant within the study population, as longitudinal motion amplitude is known to vary along the carotid artery (Zahnd, et al. 2015a). If ECG is unavailable, simultaneous measurement of the internal diameter changes over time generally helps the identification of different cycles. Moreover, analyzing the wall motion over an extended number of frames increases the risk of speckle decorrelation and loss of the tracked pattern. To address this issue, long recordings can either be analyzed cycle-by-cycle with approaches optimized for a single heartbeat (Tat, et al. 2017), or as a whole with dedicated tracking methods (Zahnd, et al. 2013).

# Discussion and conclusion

During the last decade, both the technical and clinical communities have collaborated towards the establishment of a large body of work to characterize carotid wall longitudinal motion in ultrasound. Current results enable asserting the capacity of methodological tools to obtain accurate, robust, reproducible, and (semi-) automated quantification of longitudinal motion. Furthermore, the association between several indices derived from longitudinal motion and the presence of cardiovascular risk factors shows that longitudinal motion can be a surrogate marker for atherosclerosis, and strongly suggests that this patho-physiological phenomenon is a valid candidate for vascular health assessment and putatively for early-stage cardiovascular risk prediction.

Determination of the origins of longitudinal motion pattern will greatly aid the interpretation of motion measurements for cardiovascular risk assessment. For example, discovery of passive stiffness components of the motion trace would identify a primary health outcome for future cross-sectional or interventional studies that is supported by existing conventional arterial stiffness

683 literature. Additional stimulus-response studies isolating the different phasic components of the
684 motion pattern would greatly support this research direction.

685 Building upon this knowledge, one of the leading questions to shape future studies is to determine
686 whether and how longitudinal motion quantification is appropriate to be incorporated into routine
687 clinical practice. Accordingly, it has become required to confirm the added value of longitudinal
688 motion indices in large clinical trials, including different types of subjects at risk, and a variety of
689 additional CVD markers. Such prospective trials, with long-term follow-ups, will be key to
690 identify the most robust longitudinal-motion-derived indices for disease diagnosis, prevention and
691 monitoring. The investigation of potential associations between such indices and i) other
692 ultrasound-image-based indices such as IMT and texture, and ii) disease biomarkers, such as
693 biochemical indices, will allow a more integrated and in-depth approach to arterial biomechanics.

694 Concluding, longitudinal motion is a promising yet relatively unexploited marker. By reaching out
695 to different expert communities, the aim of this review article was to raise awareness about the
696 existence of this patho-physiological phenomenon. Knowledge gathered in previous studies
697 gradually contributed to establish clinical hypotheses, as well as methodological frameworks.
698 Determining the definitive clinical applicability and added value of carotid ultrasound longitudinal
699 wall motion beyond traditional cardiovascular risk markers remains the mission of the community
700 in future explorations.

## References


Ahlgren ÅR, Cinthio M, Persson HW, Lindström K. Different patterns of longitudinal displacement of the common carotid artery wall in healthy humans are stable over a four-month period. Ultrasound in medicine & biology 2012;38:916-25.

Ahlgren ÅR, Cinthio M, Steen S, Nilsson T, Sjöberg T, Persson HW, Lindström K. Longitudinal displacement and intramural shear strain of the porcine carotid artery undergo profound changes in response to catecholamines. American Journal of Physiology-Heart and Circulatory Physiology 2011;302:H1102-H15.

Ahlgren ÅR, Cinthio M, Steen S, Persson HW, Sjöberg T, Lindström K. Effects of adrenaline on longitudinal arterial wall movements and resulting intramural shear strain: a first report. Clinical physiology and functional imaging 2009;29:353-59.

Ahlgren ÅR, Steen S, Segstedt S, Erlöv T, Lindström K, Sjöberg T, Persson HW, Ricci S, Tortoli P, Cinthio M. Profound increase in longitudinal displacements of the porcine carotid artery wall can take place independently of wall shear stress: a continuation report. Ultrasound in medicine & biology 2015;41:1342-53.

Albinsson J, Brorsson S, Ahlgren ÅR, Cinthio M. Improved Tracking Performance of Lagrangian Block-Matching Methodologies Using Block Expansion in the Time Domain: In Silico, Phantom and in Vivo Evaluations. Ultrasound in Medicine & Biology 2014;40:2508-20.

Albinsson J, Hasegawa H, Takahashi H, Boni E, Ramalli A, Rydén Ahlgren Å, Cinthio M. Iterative 2D Tissue Motion Tracking in Ultrafast Ultrasound Imaging. Applied Sciences (2076-3417) 2018;8.

Alley H, Owens CD, Gasper WJ, Grenon SM. Ultrasound assessment of endothelial-dependent flow-mediated vasodilation of the brachial artery in clinical research. JoVE (Journal of Visualized Experiments) 2014:e52070.

Au JS, Bochnak PA, Valentino SE, Cheng JL, Stöhr EJ, MacDonald MJ. Cardiac and haemodynamic influence on carotid artery longitudinal wall motion. Experimental physiology 2018a;103:141-52.

Au JS, Ditor DS, MacDonald MJ, Stöhr EJ. Carotid artery longitudinal wall motion is associated with local blood velocity and left ventricular rotational, but not longitudinal, mechanics. Physiological reports 2016;4:e12872.

Au JS, Proudfoot NA, Timmons BW, MacDonald MJ. Retrograde shift in carotid artery longitudinal wall motion after one-year follow-up in children. Atherosclerosis 2019;288:26-32.

Au JS, Shenouda N, Oikawa SY, Gillen JB, Morton RW, Gibala MJ, Phillips SM, MacDonald MJ. Carotid Artery Longitudinal Wall Motion Is Unaffected by 12 Weeks of Endurance, Sprint Interval or Resistance Exercise Training. Ultrasound in Medicine & Biology 2020;46:992-1000.

Au JS, Valentino SE, McPhee PG, MacDonald MJ. Diastolic Carotid Artery Longitudinal Wall Motion Is Sensitive to Both Aging and Coronary Artery Disease Status Independent of Arterial Stiffness. Ultrasound in Medicine & Biology 2017;43:1906-18.

Au JS, Yli-Ollila H, MacDonald MJ. An assessment of intra-individual variability in carotid artery longitudinal wall motion: recommendations for data acquisition. Physiological measurement 2018b;39:09NT01.

Basarab A, Gueth P, Liebgott H, Delachartre P. Phase-based block matching applied to motion estimation with unconventional beamforming strategies. IEEE transactions on ultrasonics, ferroelectrics, and frequency control 2009;56:945-57.

Ben-Shlomo Y, Spears M, Boustred C, May M, Anderson SG, Benjamin EJ, Boutouyrie P, Cameron J, Chen C-H, Cruickshank JK. Aortic pulse wave velocity improves cardiovascular event prediction: an individual participant meta-analysis of prospective observational data from 17,635 subjects. Journal of the American College of Cardiology 2014;63:636-46.

Chen X, Zohdy MJ, Emelianov SY, O'Donnell M. Lateral speckle tracking using synthetic lateral phase. IEEE transactions on ultrasonics, ferroelectrics, and frequency control 2004;51:540-50.

Cinthio M, Ahlgren AR, Bergkvist J, Jansson T, Persson HW, Lindstrom K. Longitudinal movements and resulting shear strain of the arterial wall. American Journal of Physiology-Heart and Circulatory Physiology 2006;291:H394-H402.

Cinthio M, Ahlgren AR, Jansson T, Eriksson A, Persson HW, Lindstrom K. Evaluation of an ultrasonic echo-tracking method for measurements of arterial wall movements in two dimensions. IEEE transactions on ultrasonics, ferroelectrics, and frequency control 2005;52:1300-11.

Cinthio M, Albinsson J, Erlöv T, Bjarnegård N, Länne T, Ahlgren ÅR. Longitudinal Movement of the Common Carotid Artery Wall: New Information on Cardiovascular Aging. Ultrasound in Medicine & Biology 2018;44:2283-95.

de Korte CL, Hansen HHG, van der Steen AFW. Vascular ultrasound for atherosclerosis imaging. Interface focus 2011;1:565-75.

Dempsey RJ, Varghese T, Jackson DC, Wang X, Meshram NH, Mitchell CC, Hermann BP, Johnson SC, Berman SE, Wilbrand SM. Carotid atherosclerotic plaque instability and cognition determined by ultrasound-measured plaque strain in asymptomatic patients with significant stenosis. Journal of neurosurgery 2018;128:111-19.

Deng S, Tomioka J, Debes J, Fung Y. New experiments on shear modulus of elasticity of arteries. American Journal of Physiology-Heart and Circulatory Physiology 1994;266:H1-H10.

Fekkes S, Saris AE, Nillesen MM, Menssen J, Hansen HH, de Korte CL. Simultaneous vascular strain and blood vector velocity imaging using high-frequency versus conventional-frequency plane wave ultrasound: A phantom study. IEEE transactions on ultrasonics, ferroelectrics, and frequency control 2018;65:1166-81.

Gamble G, Zorn J, Sanders G, MacMahon S, Sharpe N. Estimation of arterial stiffness, compliance, and distensibility from M-mode ultrasound measurements of the common carotid artery. Stroke 1994;25:11-16.

Gao Z, Li Y, Sun Y, Yang J, Xiong H, Zhang H, Liu X, Wu W, Liang D, Li S. Motion tracking of the carotid artery wall from ultrasound image sequences: a nonlinear state-space approach. IEEE transactions on medical imaging 2017a;37:273-83.

Gao Z, Sun Y, Zhang H, Ghista D, Li Y, Xiong H, Liu X, Xie Y, Wu W, Li S. 2016 Carotid Artery Wall Motion Estimated from Ultrasound Imaging Sequences Using a Nonlinear State Space Approach. *International Conference on Medical Image Computing and Computer-Assisted Intervention*: Springer, 98-106.

Gao Z, Xiong H, Liu X, Zhang H, Ghista D, Wu W, Li S. Robust estimation of carotid artery wall motion using the elasticity-based state-space approach. Medical image analysis 2017b;37:1-21.

Gao Z, Xiong H, Zhang H, Wu D, Lu M, Wu W, Wong KK, Zhang Y-T. 2015 Motion estimation of common carotid artery wall using a H∞ filter based block matching method. *International Conference on Medical Image Computing and Computer-Assisted Intervention*: Springer, 443-50.

Gastounioti A, Golemati S, Stoitsis J, Nikita K. Adaptive block matching methods for carotid artery wall motion estimation from B-mode ultrasound: in silico evaluation & in vivo application. Phys. Med. Biol 2013;58:8647-61.

Gastounioti A, Golemati S, Stoitsis J, Nikita KS. Comparison of Kalman-filter-based approaches for block matching in arterial wall motion analysis from B-mode ultrasound. Measurement Science and Technology 2011;22:114008.

Gastounioti A, Kolias V, Golemati S, Tsiaparas NN, Matsakou A, Stoitsis JS, Kadoglou NP, Gkekas C, Kakisis JD, Liapis CD. CAROTID–a web-based platform for optimal personalized management of atherosclerotic patients. Computer methods and programs in biomedicine 2014;114:183-93.

Gepner AD, Colangelo LA, Reilly N, Korcarz CE, Kaufman JD, Stein JH. Carotid artery longitudinal displacement, cardiovascular disease and risk factors: the multi-ethnic study of atherosclerosis. PloS one 2015;10:e0142138.

Gepner AD, McClelland RL, Korcarz CE, Young R, Kaufman JD, Mitchell CC, Stein JH. Carotid artery displacement and cardiovascular disease risk in the Multi-Ethnic Study of Atherosclerosis. Vascular Medicine 2019;24:405-13.

Golemati S, Gastounioti A, Nikita KS. Ultrasound-Image-Based Cardiovascular Tissue Motion Estimation. IEEE Reviews in Biomedical Engineering 2016;9:208-18.

Golemati S, Sassano A, Lever MJ, Bharath AA, Dhanjil S, Nicolaides AN. Carotid artery wall motion estimated from B-mode ultrasound using region tracking and block matching. Ultrasound in medicine & biology 2003;29:387-99.

Golemati S, Stoitsis JS, Gastounioti A, Dimopoulos AC, Koropouli V, Nikita KS. Comparison of block matching and differential methods for motion analysis of the carotid artery wall from ultrasound images. IEEE Transactions on Information Technology in Biomedicine 2012;16:852-58.
Gutierrez J, Rundek T. Carotid wall imaging, In: Baracchini C and Csiba L, eds. *Manual of Neurosonology*. Cambridge: Cambridge University Press, 2016. 34-47.
Hasegawa H. Phase-Sensitive 2D Motion Estimators Using Frequency Spectra of Ultrasonic Echoes. Applied Sciences 2016;6:195.
Hasegawa H, Kanai H. Improving accuracy in estimation of artery-wall displacement by referring to center frequency of RF echo. IEEE transactions on ultrasonics, ferroelectrics, and frequency control 2006a;53:52-63.
Hasegawa H, Kanai H. Modification of the phased-tracking method for reduction of artifacts in estimated artery wall deformation. ieee transactions on ultrasonics, ferroelectrics, and frequency control 2006b;53.
Hasegawa H, Kanai H. Reduction of influence of variation in center frequencies of RF echoes on estimation of artery-wall strain. IEEE Transactions on Ultrasonics, Ferroelectrics, and Frequency Control 2008a;55:1921-34.
Hasegawa H, Kanai H. Simultaneous imaging of artery-wall strain and blood flow by high frame rate acquisition of RF signals. IEEE transactions on ultrasonics, ferroelectrics, and frequency control 2008b;55:2626-39.
Hasegawa H, Kanai H. Phase-sensitive lateral motion estimator for measurement of artery-wall displacement-phantom study. IEEE transactions on ultrasonics, ferroelectrics, and frequency control 2009;56.
Hein I, O'brien WD. Current time-domain methods for assessing tissue motion by analysis from reflected ultrasound echoes-a review. IEEE transactions on ultrasonics, ferroelectrics, and frequency control 1993;40:84-102.
Horn BK, Schunck BG. Determining optical flow. Artificial intelligence 1981;17:185-203.
Humphrey J, Eberth J, Dye W, Gleason R. Fundamental role of axial stress in compensatory adaptations by arteries. Journal of biomechanics 2009;42:1-8.
Idzenga T, Hansen HH, Thijssen JM, de Korte CL. Enhancing the performance of lateral shear strain estimation by using 2-D strain imaging. IEEE transactions on ultrasonics, ferroelectrics, and frequency control 2014;61:756-64.
Jensen JA. 1996 Field: A program for simulating ultrasound systems. *10TH NORDICBALTIC CONFERENCE ON BIOMEDICAL IMAGING, VOL. 4, SUPPLEMENT 1, PART 1: 351--353*: Citeseer.
Jensen JA, Munk P. A new method for estimation of velocity vectors. IEEE transactions on ultrasonics, ferroelectrics, and frequency control 1998;45:837-51.
Kasai C, Namekawa K, Koyano A, Omoto R. Real-time two-dimensional blood flow imaging using an autocorrelation technique. IEEE Transactions on sonics and ultrasonics 1985;32:458-64.
Lawton R, Greene L. A method for the in situ study of aortic elasticity in the dog. Authorized Medical Allowance List, US Naval and Air Development Center, Warminister, PA (Rep. No. NADC-MA-5603) 1956.
Liebgott H, Basarab A, Gueth P, Friboulet D, Delachartre P. Transverse oscillations for tissue motion estimation. Ultrasonics 2010;50:548-55.
Liebgott H, Wilhjelm JE, Jensen JA, Vray D, Delachartre P. PSF dedicated to estimation of displacement vectors for tissue elasticity imaging with ultrasound. ieee transactions on ultrasonics, ferroelectrics, and frequency control 2007;54:746-56.
Lopata RGP, Nillesen MM, Hansen HHG, Gerrits IH, Thijssen JM, de Korte CL. Performance Evaluation of Methods for Two-Dimensional Displacement and Strain Estimation Using Ultrasound Radio Frequency Data. Ultrasound in Medicine and Biology 2009;35:796-812.
Makūnaitė M, Jurkonis R, Rodríguez-Martínez A, Jurgaitienė R, Semaška V, Mėlinytė K, Kubilius R. Ultrasonic Parametrization of Arterial Wall Movements in Low- and High-Risk CVD Subjects. Applied Sciences 2019;9:465.
Miyajo A, Hasegawa H. Comparison of method using phase-sensitive motion estimator with speckle tracking method and application to measurement of arterial wall motion. Japanese Journal of Applied Physics 2018;57:07LF11.

Miyajo A, Nagaoka R, Hasegawa H. Comparison of ultrasonic motion estimators for vascular applications. Japanese Journal of Applied Physics 2019;58:SGGE16.
Mozaffarian D, Benjamin EJ, Go AS, Arnett DK, Blaha MJ, Cushman M, Das SR, de Ferranti S, Després J-P, Fullerton HJ. Heart disease and stroke statistics—2016 update: a report from the American Heart Association. Circulation 2015:CIR. 0000000000000350.
Murray V, Murillo S, Pattichis M, Loizou C, Pattichis C, Kyriacou E, Nicolaides A. 2007 An AM-FM model for motion estimation in atherosclerotic plaque videos. *Signals, Systems and Computers, 2007. ACSSC 2007. Conference Record of the Forty-First Asilomar Conference on*: IEEE, 746-50.
Nichols W, Rourke M, Hartley C. McDonald s Blood Flow in Arteries: Theoretical, experimental and clinical principles. Arnold and Oxford University Press Inc. New York, London, Sydney, Auckland 1997.
Nilsson T, Ahlgren ÅR, Jansson T, Persson HW, Nilsson J, Lindström K, Cinthio M. 2010 A method to measure shear strain with high spatial resolution in the arterial wall non-invasively in vivo by tracking zero-crossings of B-mode intensity gradients. *Ultrasonics Symposium (IUS), 2010 IEEE*: IEEE, 491-94.
Patel DJ, Fry DL, Janicki JS. The elastic symmetry of arterial segments in dogs. Circulation research 1969;24:1-8.
Patel DJ, Mallos AJ, Fry DL. Aortic mechanics in the living dog. Journal of Applied Physiology 1961;16:293-99.
Perrot V, Liebgott H, Long A, Vray D. 2018a Simultaneous Tissue and Flow Estimation at High Frame Rate Using Plane Wave and Transverse Oscillation on in Vivo Carotid. *2018 IEEE International Ultrasonics Symposium (IUS)*, 1-4.
Perrot V, Petrusca L, Bernard A, Vray D, Liebgott H. 2017 Simultaneous pulse wave and flow estimation at high-framerate using plane wave and transverse oscillation on carotid phantom. *2017 IEEE International Ultrasonics Symposium (IUS)*: IEEE, 1-4.
Perrot V, Salles S, Vray D, Liebgott H. Video Magnification Applied in Ultrasound. IEEE Transactions on Biomedical Engineering 2018b;66:283-88.
Persson M, Rydén Ahlgren Å, Jansson T, Eriksson A, Persson HW, Lindström K. A new non- invasive ultrasonic method for simultaneous measurements of longitudinal and radial arterial wall movements: first in vivo trial. Clinical physiology and functional imaging 2003;23:247-51.
Proudfoot NA, Au JS, Timmons BW, MacDonald MJ. Associations between carotid artery longitudinal wall motion and arterial stiffness indicators in young children. Atherosclerosis 2019.
Qorchi S, Zahnd G, Galbrun D, Sérusclat A, Moulin P, Vray D, Orkisz M. Kalman-Based Carotid-Artery Longitudinal-Kinetics Estimation and Pattern Recognition. Innovation and Researchin BioMedical Engineering 2017;38:219-23.
Ribbers H, Lopata RG, Holewijn S, Pasterkamp G, Blankensteijn JD, De Korte CL. Noninvasive two-dimensional strain imaging of arteries: validation in phantoms and preliminary experience in carotid arteries in vivo. Ultrasound in medicine & biology 2007;33:530-40.
Rizi FY, Setarehdan SK, Behnam H. Measuring the effect of aging on vibrations of the carotid artery wall using empirical mode decomposition method. Journal of medical signals and sensors 2014;4:27.
Rusconi C, Raddino R, Trichaki E, Dei Cas L. Atherosclerotic Plaque Regression and Arterial Reverse Remodelling in Carotid and Femoral Arteries by Statin Use in Primary Prevention Setting: Ultrasound Findings. *Ultrasound Imaging-Medical Applications*: IntechOpen, 2011.
Salles S, Chee AJ, Garcia D, Alfred C, Vray D, Liebgott H. 2-D arterial wall motion imaging using ultrafast ultrasound and transverse oscillations. IEEE transactions on ultrasonics, ferroelectrics, and frequency control 2015;62:1047-58.
Salles S, Zahnd G, Liebgott H, Sérusclat A, Vray D. 2012 Real time US-tagging combined with phase-based optical flow applied to 2D motion estimation of the carotid artery wall. *Ultrasonics Symposium (IUS), 2012 IEEE International*: IEEE, 1185-88.
Scaramuzzino S, Carallo C, Pileggi G, Gnasso A, Spadea MF. Longitudinal motion assessment of the carotid artery using speckle tracking and scale-invariant feature transform. Annals of biomedical engineering 2017;45:1865-76.
Shi H, Mitchell CC, McCormick M, Kliewer MA, Dempsey RJ, Varghese T. Preliminary in vivo atherosclerotic carotid plaque characterization using the accumulated axial strain and relative lateral shift strain indices. Physics in Medicine & Biology 2008;53:6377.

Shi H, Varghese T. Two-dimensional multi-level strain estimation for discontinuous tissue. Physics in Medicine & Biology 2007;52:389.
Simonson JS, Schiller NB. Descent of the base of the left ventricle: an echocardiographic index of left ventricular function. J Am Soc Echocardiogr 1989;2:25-35.
Soleimani E, Mokhtari-Dizaji M, Saberi H, Sharif-Kashani S. A mathematical model for estimating the axial stress of the common carotid artery wall from ultrasound images. Medical & biological engineering & computing 2016;54:1205-15.
Stoitsis J, Golemati S, Dimopoulos A, Nikita K. 2006 Analysis and quantification of arterial wall motion from B-mode ultrasound images-comparison of block-matching and optical flow. *Engineering in Medicine and Biology Society, 2005. IEEE-EMBS 2005. 27th Annual International Conference of the*: IEEE, 4469-72.
Sumi C. Displacement vector measurement using instantaneous ultrasound signal phase-multidimensional autocorrelation and Doppler methods. IEEE transactions on ultrasonics, ferroelectrics, and frequency control 2008;55:24-43.
Svedlund S, Eklund C, Robertsson P, Lomsky M, Gan L-M. Carotid artery longitudinal displacement predicts 1-year cardiovascular outcome in patients with suspected coronary artery disease. Arteriosclerosis, Thrombosis, and Vascular Biology 2011;31:1668-74.
Svedlund S, Gan L-m. Longitudinal common carotid artery wall motion is associated with plaque burden in man and mouse. Atherosclerosis 2011a;217:120-24.
Svedlund S, Gan LM. Longitudinal wall motion of the common carotid artery can be assessed by velocity vector imaging. Clinical physiology and functional imaging 2011b;31:32-38.
Swillens A, De Santis G, Degroote J, Lovstakken L, Vierendeels J, Segers P. Accuracy of carotid strain estimates from ultrasonic wall tracking: A study based on multiphysics simulations and in vivo data. IEEE transactions on medical imaging 2011;31:131-39.
Taivainen SH, Yli-Ollila H, Juonala M, Kahonen M, Raitakari OT, Laitinen TM, Laitinen TP. Interrelationships between indices of longitudinal movement of the common carotid artery wall and the conventional measures of subclinical arteriosclerosis. Clin Physiol Funct Imaging 2017;37:305-13.
Taivainen SH, Yli-Ollila H, Juonala M, Kähönen M, Raitakari OT, Laitinen TM, Laitinen TP. Influence of cardiovascular risk factors on longitudinal motion of the common carotid artery wall. Atherosclerosis 2018;272:54-59.
Tat J, Au JS, Keir PJ, MacDonald MJ. Reduced common carotid artery longitudinal wall motion and intramural shear strain in individuals with elevated cardiovascular disease risk using speckle tracking. Clin Physiol Funct Imaging 2017;37:106-16.
Tat J, Psaromiligkos IN, Daskalopoulou SS. Carotid atherosclerotic plaque alters the direction of longitudinal motion in the artery wall. Ultrasound in medicine & biology 2016;42:2114-22.
Thijssen DH, Black MA, Pyke KE, Padilla J, Atkinson G, Harris RA, Parker B, Widlansky ME, Tschakovsky ME, Green DJ. Assessment of flow-mediated dilation in humans: a methodological and physiological guideline. American Journal of Physiology-Heart and Circulatory Physiology 2010;300:H2-H12.
Touboul P-J. Intima-media thickness of carotid arteries. *Translational Neurosonology*: Karger Publishers, 2015. 31-39.
Touboul PJ, Hennerici MG, Meairs S, Adams H, Amarenco P, Bornstein N, Csiba L, Desvarieux M, Ebrahim S, Hernandez Hernandez R, Jaff M, Kownator S, Naqvi T, Prati P, Rundek T, Sitzer M, Schminke U, Tardif JC, Taylor A, Vicaut E, Woo KS. Mannheim carotid intima-media thickness and plaque consensus (2004-2006-2011). An update on behalf of the advisory board of the 3rd, 4th and 5th watching the risk symposia, at the 13th, 15th and 20th European Stroke Conferences, Mannheim, Germany, 2004, Brussels, Belgium, 2006, and Hamburg, Germany, 2011. Cerebrovasc Dis 2012;34:290-6.
Townsend RR, Wilkinson IB, Schiffrin EL, Avolio AP, Chirinos JA, Cockcroft JR, Heffernan KS, Lakatta EG, McEniery CM, Mitchell GF. Recommendations for improving and standardizing vascular research on arterial stiffness: a scientific statement from the American Heart Association. Hypertension 2015;66:698-722.

968 Tozzi P, Hayoz D, Oedman C, Mallabiabarrena I, Von Segesser L. Systolic axial artery length reduction:
969 an overlooked phenomenon in vivo. American Journal of Physiology-Heart and Circulatory
970 Physiology 2001;280:H2300-H05.
971 Van Bortel LM, Laurent S, Boutouyrie P, Chowienczyk P, Cruickshank J, De Backer T, Filipovsky J,
972 Huybrechts S, Mattace-Raso FU, Protogerou AD. Expert consensus document on the measurement
973 of aortic stiffness in daily practice using carotid-femoral pulse wave velocity. Journal of
974 hypertension 2012;30:445-48.
975 Vlachopoulos C, O'Rourke M, Nichols WW. McDonald's blood flow in arteries: theoretical, experimental
976 and clinical principles: CRC press, 2011.
977 Yli-Ollila H, Laitinen T, Weckström M, Laitinen T. Axial and radial waveforms in common carotid artery:
978 An advanced method for studying arterial elastic properties in ultrasound imaging. Ultrasound in
979 medicine & biology 2013;39:1168-77.
980 Yli-Ollila H, Tarvainen MP, Laitinen TP, Laitinen TM. Principal component analysis of the longitudinal
981 carotid wall motion in association with vascular stiffness: a pilot study. Ultrasound in medicine &
982 biology 2016a;42:2873-86.
983 Yli-Ollila H, Tarvainen MP, Laitinen TP, Laitinen TM. Transfer Function Analysis of the Longitudinal
984 Motion of the Common Carotid Artery Wall. Frontiers in Physiology 2016b;7.
985 Yousefi Rizi F, Setarehdan SK, Behnam H, Alizadeh Sani Z. Study of the effects of age and body mass
986 index on the carotid wall vibration: Extraction methodology and analysis. Proceedings of the
987 Institution of Mechanical Engineers, Part H: Journal of Engineering in Medicine 2014;228:714-29.
988 Zahnd G, Balocco S, Sérusclat A, Moulin P, Orkisz M, Vray D. Progressive attenuation of the longitudinal
989 kinetics in the common carotid artery: preliminary in vivo assessment. Ultrasound Med Biol
990 2015a;41:339-45.
991 Zahnd G, Boussel L, Sérusclat A, Vray D. 2011a Intramural shear strain can highlight the presence of
992 atherosclerosis: a clinical in vivo study. *2011 IEEE International Ultrasonics Symposium*: IEEE,
993 1770-73.
994 Zahnd G, Boussel S, Sérusclat A, Moulin P, Orkisz M, Vray D. Measurement of two-dimensional
995 movement parameters of the carotid artery wall for early detection of arteriosclerosis: a preliminary
996 clinical study. Ultrasound in Medicine & Biology 2011b;37:1421-29.
997 Zahnd G, Galbrun D, Qorchi S, Saito K, Sérusclat A, Moulin P, Nagatsuka K, Orkisz M, Otake Y, Sato Y.
998 2017a Pattern Analysis of the Kinematics in Ultrasound Videos of the Common Carotid Artery–
999 Application to Cardiovascular Risk Evaluation. *International Forum on Medical Imaging in Asia*
1000 *(IFMIA 2017)*.
1001 Zahnd G, Kapellas K, van Hattem M, van Dijk A, Serusclat A, Moulin P, van der Lugt A, Skilton M, Orkisz
1002 M. A Fully-Automatic Method to Segment the Carotid Artery Layers in Ultrasound Imaging:
1003 Application to Quantify the Compression-Decompression Pattern of the Intima-Media Complex
1004 During the Cardiac Cycle. Ultrasound Med Biol 2017b;43:239-57.
1005 Zahnd G, Orkisz M, Dávila Serrano EE, Vray D. 2019 CAROLAB – A platform to analyze carotid
1006 ultrasound data. *IEEE Ultrasonics Symposium*. Glasgow (Scotland).
1007 Zahnd G, Orkisz M, Sérusclat A, Moulin P, Vray D. Evaluation of a Kalman-based block matching method
1008 to assess the bi-dimensional motion of the carotid artery wall in B-mode ultrasound sequences.
1009 Medical Image Analysis 2013;17:573-85.
1010 Zahnd G, Saito K, Nagatsuka K, Otake Y, Sato Y. Dynamic Block Matching to assess the longitudinal
1011 component of the dense motion field of the carotid artery wall in B-mode ultrasound sequences -
1012 Association with coronary artery disease. Medical physics 2018.
1013 Zahnd G, Salles S, Liebgott H, Vray D, Sérusclat A, Moulin P. Real-time ultrasound-tagging to track the
1014 2D motion of the common carotid artery wall in vivo. Medical Physics 2015b;42:820-30.
1015 Zahnd G, Vray D, Sérusclat A, Alibay D, Bartold M, Brown A, Durand M, Jamieson LM, Kapellas K,
1016 Maple-Brown LJ. Longitudinal displacement of the carotid wall and cardiovascular risk factors:
1017 associations with aging, adiposity, blood pressure and periodontal disease independent of cross-
1018 sectional distensibility and intima-media thickness. Ultrasound in medicine & biology
1019 2012;38:1705-15.
1020 Zambacevičienė M, Jurkonis R. 2019 RF Ultrasound Based Longitudinal Motion Estimation of Carotid
1021 Artery Wall: Feasibility Study. *World Congress on Medical Physics and Biomedical Engineering*
1022 *2018*: Springer, 253-57.

1023 Zhang L, Yin J-K, Duan Y-Y, Liu X, Xu L, Wang J, Yang Y-L, Yuan L-J, Cao T-S. Evaluation of carotid
1024 artery elasticity changes in patients with type 2 diabetes. Cardiovascular diabetology 2014;13:39.

1025

# Tables

Table 1. Wall motion extraction techniques based on B-mode ultrasound imaging (chronological order).

| Study | Year | Technique | Data | Accuracy evaluation | |
|---|---|---|---|---|---|
| | | | | Criteria | Score |
| Golemati et al. (Golemati, et al. 2003) | 2003 | Block Matching (BM) | 11 symptomatic subjects<br>9 asymptomatic subjects | No quantitative evaluation of the accuracy | - |
| Persson et al. (Persson, et al. 2003) | 2003 | Echo tracking | 1 healthy volunteer | No quantitative evaluation of the accuracy | - |
| Cinthio et al. (Cinthio, et al. 2005) | 2005 | Echo tracking | 1 healthy volunteer<br>1 agar phantom | Mean differences compared with two high-resolution triangulation lasers. | Longitudinal: 5.9±40.5 μm<br>Radial: 28.5±19.5 μm |
| Stoitsis et al. (Stoitsis, et al. 2006) | 2006 | BM & Optical Flow (OF) | 10 healthy volunteers | Cross-correlation coefficient between BM and OF | Longitudinal:0.32±0.39 mm<br>Radial:0.72±0.22 mm |
| Gastounioti et al. (Gastounioti, et al. 2011) | 2011 | BM + Kalman filtering as an adaptive strategy with (a) updating the reference block (b) updating the displacements | 5 young healthy volunteers (ages: 25–32 years)<br>4 elderly healthy volunteers (ages: 44–73 years) | Tracking accuracy compared to conventional BM | Adaptive BM minimized the warping index and yielded average displacement error reductions of 24% with respect to BM.<br>Estimation bias reduction of 30% with respect to BM.<br>Jitter over varying center frequencies reduction of 64% with respect to BM. |
| Zahnd et al. (Zahnd, et al. 2011b) | 2011 | Multi-BM ruled by a deformable skeleton model | 26 young healthy volunteers<br>26 elderly diabetic subjects | Qualitative evaluation only (visual control by two experts) | - |
| Golemati et al. (Golemati, et al. 2012) | 2012 | Comparison of several existing methods: OF, weighted least-squares OF (WLSOF), BM, and affine block motion model (ABMM) | Real image template and Field II | Average warping indices between OF, WLOF, BM and ABMM | WLSOF: 105 μm<br>ABMM: 120 μm<br>BM: 405 μm<br>OF: 694 μm |
| Salles et al. (Salles, et al. 2012) | 2012 | Phase-based OF | 1 healthy volunteer | Qualitative evaluation only | - |
| Zahnd et al. (Zahnd, et al. 2012) | 2012 | Multi-BM guided by contour segmentation | 126 Indigenous Australians with periodontal disease<br>27 healthy age- and sex-matched Caucasian controls | Qualitative evaluation only (visual control by two experts) | - |
| Zahnd et al. (Zahnd, et al. 2013) | 2013 | Kalman-based BM | 57 young healthy volunteers<br>25 diabetic patients | Average absolute error (±STD) from manual reference tracings | Longitudinal =20±19 μm<br>Radial=84±107 μm |
| Gastounioti et al. (Gastounioti, et al. 2013) | 2013 | Adaptive BM | 40 subjects<br>1 in silico phantom | Tracking accuracy compared to conventional BM | Adaptive BM algorithm, yielding a 47% accuracy increase with respect to the conventional BM |

| | | | | | |
|---|---|---|---|---|---|
| Yli-Ollila et al. (Yli-Ollila, et al. 2013) | 2013 | BM + luminance optimization | 19 healthy volunteers | Reproducibility | Cronbach's α coefficient, 0.59–0.97 |
| Albinsson et al. (Albinsson, et al. 2014) | 2014 | Lagrangian BM | 20 healthy volunteers<br>1 Simulated (Field II (Jensen 1996))<br>1 in silico phantom | Absolute tracking error compared to Cinthio et al. (Cinthio, et al. 2005) | In silico: improvement of tracking accuracy (mean=48%, p<0.005)<br>Phantom: improvement of tracking accuracy (mean=43%, p<0.01)<br>In vivo: reduction of block size with similar tracking performance (mean=19%, p<0.01 |
| Gao et al. (Gao, et al. 2015) | 2015 | BM + h∞ filter | 50 subjects | Mean absolute tracking difference compared with manual annotations | Mean absolute estimation error:<br>Longitudinal 96 μm<br>Radial 46 μm |
| Salles et al. (Salles, et al. 2012) | 2015 | Phase-based BM | 1 simulated RF clip (FieldII)<br>10 healthy volunteers | Mean absolute amplitude difference, evaluated on a numerical phantom | Longitudinal: 9.9±7.9 μm<br>Radial: 4.2±3.4 μm |
| Yli-Ollila et al. (Yli-Ollila, et al. 2016b) | 2016 | Transfer function analysis | 19 healthy volunteers | Reproducibility | Longitudinal: Cronbach's α coefficient, 0.59–0.97<br>Radial: Cronbach's α coefficient, 0.68–0.93 |
| Tat et al. (Tat, et al. 2016) | 2016 | Multi-BM | 23 healthy volunteers<br>12 patients | Not specified | - |
| Gao et al. (Gao, et al. 2017b) | 2017 | Elasticity-based state-space approach | 37 healthy volunteers<br>103 patients | Correlation coefficient (r) and root mean square error (RMSE) against manual tracings | Radial: r = 0.9897, RMSE= 25.98 μm<br>Longitudinal: r=0.9536, RMSE= 142.82 μm |
| Scaramuzzino et al. (Scaramuzzino, et al. 2017) | 2017 | Automatic detection and matching of multiple salient points + Scale invariant feature transform | 1 in silico phantom<br>18 healthy volunteers<br>16 patients | Accuracy<br>Average absolute error (±STD), Maximum variation<br>Coefficient, Correlation coefficient | In silico:<br>Intima-media complex: 23±15 μm<br>Adventitia: 19±18 μm<br>In vivo:<br>Intima-media complex: 9.5 (variation coefficient, over 5 repeated measures)<br>Adventitia: 13.8% (variation coefficient, over 5 repeated measures)<br>Compared with visual assessment performed by 2 physicians: r= 0.7 |
| Gao et. al. (Gao, et al. 2017a) | 2017 | Nonlinear state space with a time-variant control signal based on a mathematical model of the carotid dynamics | 30 simulated sequences<br>22 healthy volunteers<br>81 patients | Intra-class correlation | In silico: accuracy 0.1161─0.1260 mm<br>In vivo:<br>Longitudinal:<br>Intra-class correlation ≥0.9948<br>95% CI = 0.8871 mm<br>Radial:<br>Intra-class correlation ≥0.9966 95% CI = 0.4159 mm |
| Zahnd et al. (Zahnd, et al. 2018) | 2018 | Dynamic BM | 62 elderly patients at high cardiovascular risk | Average absolute error (±STD) from manual reference tracings | 150±163 μm |
| Albinsson et al. (Albinsson, et al. 2018) | 2018 | Parabolic sub-sample and grid slope sub-sample interpolation for 2D BM | 1 healthy volunteer<br>1 phantom<br>1 in silico simulation (Filed II) | Absolute sub-sample estimation errors | Reduced by 24% on phantom data<br>Reduced by 15% on in silico data |

1026

1027

1028

1029

Table 2. Wall motion extraction techniques based on RF ultrasound signals (chronological order).

| **Study** | **Year** | **Technique** | **Hardware, format of RF data** | **Data** | **Performance** |
|---|---|---|---|---|---|
| Ribbers et al. (Ribbers, et al. 2007) | 2007 | Cross correlation | fr=25Hz, fs=39MHz, fc=11MHz, 15-6L linear array Philips Sonos 7500 real-time 3D echoscannerB | 1 physical phantom 12 patients | No quantitative analysis of the *in vivo* results was performed. |
| Zahnd et al. (Zahnd, et al. 2015b) | 2015 | Local Phase-Based OF (Basarab, et al. 2009) | fr=91Hz fs=50MHz, fc=4MHz, fs50MHZ, ULA-OP research scanner, | 20 young healthy volunteers 6 elderly patients | Longitudinal: 98±84 μm Radial: 55±44 μm |
| Salles et al. (Salles, et al. 2015) | 2015 | Transverse oscillations (Liebgott, et al. 2010) | fr=10kHz fc=5MHz fs=40MHz L14-5W/60 array Ultrasonix SonixTouch US system (Richmond, BC, Canada) | - 3 artery numerical phantoms | Mean axial error: 4.2 ± 3.4 μm Mean lateral errors: 9.9 ± 7.9 μm the stiffnesses of the 3 vessel phantom walls investigated were estimated with an average relative error of 2.2%. |
| Hasegawa et al. (Hasegawa 2016) | 2016 | Phase tracking with frequency spectra | fr=1302Hz fs=31.25 MHz fc=7.5MHz linear array PU-0558, Ueda Japan Radio) (scanner RSYS0002, Microsonic, Tokyo, Japan) | 1 phantom | Bias error 1D: Ra=11.5%, Lo=2.0% Bias Error 2D: Ra= 3.0%, Lo= 2.0% |
| Zambacevičienė et al. (Zambacevičienė and Jurkonis 2019) | 2018 | Phase correlation and sub-sample algorithm | fr=52Hz fs=40MHz fc=14-5 MHz Linear array Scanner Ultrasonix sonixTouch (Analogic Ultrasound, Canada) | 1 phantom | NRMSE of detected motion amplitude: 0.21 to 0.41 μm and the coefficient of correlation-= 0.95 to 0.98 in case of any determined longitudinal motion function when the phase correlation, sub-pixel algorithm and additional filtering were used. |
| Miyajo et al. (Miyajo and Hasegawa 2018) | 2018 | Matching performed in the 2D Fourier domain | Scanner α-10, Aloka. fr=3472Hz fs=40MHz fc=10MHz | 1 phantom 1 healthy volunteer | Bias error and standard deviation in the lateral velocity estimates: 0.048 and 0.282mm/s |
| Perrot et al. (Perrot, et al. 2018b) | 2018 | Video magnification | fr=2500Hz fs=25MHz fc= 5MHz Linear array (L7-4 ) (Scanner Verasonics Inc., Redmond, WA, USA) Reconstruction technique: Stolts | 8 healthy volunteers | Motion magnification by a factor 1000 |

NRMSE= normalized root mean square error; fr=Frame rate, fs= Sample Frequency, fc=Center Frequency

1030

# Figure Captions List

Figure 1: Carotid wall longitudinal motion observed in ultrasound. (a) B-mode image of the common carotid artery. (b) Detailed region of the white rectangle in (a), showing the concentric anatomical layers. (c) Schematic representation of the general waveform pattern of longitudinal motion, corresponding to the white dot in (a), over three cardiac cycles. Here, positive curve deflections represent motion in the same direction as the blood flow. A1: first anterograde motion. R: retrograde motion. A2: second anterograde motion. Δ: peak-to-peak amplitude, generally corresponding to 0.5–1 mm. The electrocardiogram (ECG) signal is schematized on the bottom. The dashed line represents the zero level, which is arbitrarily placed by convention at the time-point of the ECG R-peak (when ECG is unavailable, the zero level can be placed at the time-point where the lumen diameter is minimal).

Figure 2 - Different patterns of longitudinal motion (solid line) of the IM (intima-media) of the carotid artery far wall, and the diameter change (dashed line). a) Backward-oriented Type I (29-year-old man), b) Type II (29-year-old woman), c) Forward-oriented Type III (20-year-old woman), d) Backward-oriented type IV pattern III (55-year-old woman), e) Backward-oriented type I/IV pattern (60-year-old man), f) Forward oriented type V pattern (62-year-old woman). Small circles mark the onset of the anterograde phase A in early systole. (Source: (Cinthio, et al. 2018))

Figure 3- (a) Biaxial hysteresis loop of wall displacement, at baseline (solid) and follow-up (dashed). Biaxial wall displacement starts at the reference position [0,0], with arrows indicating the direction of motion over time and the relative phase of the longitudinal motion trace. Motion traces were interpolated to a single cardiac cycle to present data as a group average for the entire sample. (b) Corresponding longitudinal motion (Source: (Au, et al. 2018b))

# Tables

Table 1. Wall motion extraction techniques based on B-mode ultrasound imaging (chronological order).

| Study | Year | Technique | Data | Accuracy evaluation | |
|---|---|---|---|---|---|
| | | | | Criteria | Score |
| Golemati et al. (Golemati, et al. 2003) | 2003 | Block Matching (BM) | 11 symptomatic subjects<br>9 asymptomatic subjects | No quantitative evaluation of the accuracy | - |
| Persson et al. (Persson, et al. 2003) | 2003 | Echo tracking | 1 healthy volunteer | No quantitative evaluation of the accuracy | - |
| Cinthio et al. (Cinthio, et al. 2005) | 2005 | Echo tracking | 1 healthy volunteer<br>1 agar phantom | Mean differences compared with two high-resolution triangulation lasers. | Longitudinal: 5.9±40.5 μm<br>Radial: 28.5±19.5 μm |
| Stoitsis et al. (Stoitsis, et al. 2006) | 2006 | BM & Optical Flow (OF) | 10 healthy volunteers | Cross-correlation coefficient between BM and OF | Longitudinal:0.32±0.39 mm<br>Radial:0.72±0.22 mm |
| Gastounioti et al. (Gastounioti, et al. 2011) | 2011 | BM + Kalman filtering as an adaptive strategy with (a) updating the reference block (b) updating the displacements | 5 young healthy volunteers (ages: 25–32 years)<br>4 elderly healthy volunteers (ages: 44–73 years) | Tracking accuracy compared to conventional BM | Adaptive BM minimized the warping index and yielded average displacement error reductions of 24% with respect to BM.<br>Estimation bias reduction of 30% with respect to BM.<br>Jitter over varying center frequencies reduction of 64% with respect to BM. |
| Zahnd et al. (Zahnd, et al. 2011b) | 2011 | Multi-BM ruled by a deformable skeleton model | 26 young healthy volunteers<br>26 elderly diabetic subjects | Qualitative evaluation only (visual control by two experts) | - |
| Golemati et al. (Golemati, et al. 2012) | 2012 | Comparison of several existing methods: OF, weighted least-squares OF (WLSOF), BM, and affine block motion model (ABMM) | Real image template and Field II | Average warping indices between OF, WLOF, BM and ABMM | WLSOF: 105 μm<br>ABMM: 120 μm<br>BM: 405 μm<br>OF: 694 μm |
| Salles et al. (Salles, et al. 2012) | 2012 | Phase-based OF | 1 healthy volunteer | Qualitative evaluation only | - |
| Zahnd et al. (Zahnd, et al. 2012) | 2012 | Multi-BM guided by contour segmentation | 126 Indigenous Australians with periodontal disease<br>27 healthy age- and sex-matched Caucasian controls | Qualitative evaluation only (visual control by two experts) | - |
| Zahnd et al. (Zahnd, et al. 2013) | 2013 | Kalman-based BM | 57 young healthy volunteers<br>25 diabetic patients | Average absolute error (±STD) from manual reference tracings | Longitudinal =20±19 μm<br>Radial=84±107 μm |

| | | | | | |
|---|---|---|---|---|---|
| Gastounioti et al. (Gastounioti, et al. 2013) | 2013 | Adaptive BM | 40 subjects<br>1 in silico phantom | Tracking accuracy compared to conventional BM | Adaptive BM algorithm, yielding a 47% accuracy increase with respect to the conventional BM |
| Yli-Ollila et al. (Yli-Ollila, et al. 2013) | 2013 | BM + luminance optimization | 19 healthy volunteers | Reproducibility | Cronbach's α coefficient, 0.59–0.97 |
| Albinsson et al. (Albinsson, et al. 2014) | 2014 | Lagrangian BM | 20 healthy volunteers<br>1 Simulated (Field II (Jensen 1996))<br>1 in silico phantom | Absolute tracking error compared to Cinthio et al. (Cinthio, et al. 2005) | In silico: improvement of tracking accuracy (mean=48%, $p<0.005$)<br>Phantom: improvement of tracking accuracy (mean=43%, $p<0.01$)<br>In vivo: reduction of block size with similar tracking performance (mean=19%, $p<0.01$ |
| Gao et al. (Gao, et al. 2015) | 2015 | BM + h∞ filter | 50 subjects | Mean absolute tracking difference compared with manual annotations | Mean absolute estimation error:<br>Longitudinal 96 μm<br>Radial 46 μm |
| Salles et al. (Salles, et al. 2012) | 2015 | Phase-based BM | 1 simulated RF clip (FieldII)<br>10 healthy volunteers | Mean absolute amplitude difference, evaluated on a numerical phantom | Longitudinal: 9.9±7.9 μm<br>Radial: 4.2±3.4 μm |
| Yli-Ollila et al. (Yli-Ollila, et al. 2016b) | 2016 | Transfer function analysis | 19 healthy volunteers | Reproducibility | Longitudinal: Cronbach's α coefficient, 0.59–0.97<br>Radial: Cronbach's α coefficient, 0.68–0.93 |
| Tat et al. (Tat, et al. 2016) | 2016 | Multi-BM | 23 healthy volunteers<br>12 patients | Not specified | - |
| Gao et al. (Gao, et al. 2017b) | 2017 | Elasticity-based state-space approach | 37 healthy volunteers<br>103 patients | Correlation coefficient (r) and root mean square error (RMSE) against manual tracings | Radial: r = 0.9897, RMSE= 25.98 μm<br>Longitudinal: r=0.9536, RMSE= 142.82 μm |
| Scaramuzzino et al. (Scaramuzzino, et al. 2017) | 2017 | Automatic detection and matching of multiple salient points + Scale invariant feature transform | 1 in silico phantom<br>18 healthy volunteers<br>16 patients | Accuracy<br>Average absolute error (±STD), Maximum variation<br>Coefficient, Correlation coefficient | In silico:<br>Intima-media complex: 23±15 μm<br>Adventitia: 19±18 μm<br>In vivo:<br>Intima-media complex: 9.5 (variation coefficient, over 5 repeated measures)<br>Adventitia: 13.8% (variation coefficient, over 5 repeated measures)<br>Compared with visual assessment performed by 2 physicians: r= 0.7 |
| Gao et. al. (Gao, et al. 2017a) | 2017 | Nonlinear state space with a time-variant control signal based on a mathematical model of the carotid dynamics | 30 simulated sequences<br>22 healthy volunteers<br>81 patients | Intra-class correlation | In silico: accuracy 0.1161─0.1260 mm<br>In vivo:<br>Longitudinal:<br>Intra-class correlation ≥0.9948<br>95% CI = 0.8871 mm<br>Radial:<br>Intra-class correlation ≥0.9966 95% CI = 0.4159 mm |
| Zahnd et al. (Zahnd, et al. 2018) | 2018 | Dynamic BM | 62 elderly patients at high cardiovascular risk | Average absolute error (±STD) from manual reference tracings | 150±163 μm |
| Albinsson et al. (Albinsson, et al. 2018) | 2018 | Parabolic sub-sample and grid slope sub-sample interpolation for 2D BM | 1 healthy volunteer<br>1 phantom<br>1 in silico simulation (Filed II) | Absolute sub-sample estimation errors | Reduced by 24% on phantom data<br>Reduced by 15% on in silico data |

Table 2. Wall motion extraction techniques based on RF ultrasound signals (chronological order).

| **Study** | **Year** | **Technique** | **Hardware, format of RF data** | **Data** | **Performance** |
|---|---|---|---|---|---|
| Ribbers et al. (Ribbers, et al. 2007) | 2007 | Cross correlation | fr=25Hz,<br>fs=39MHz,<br>fc=11MHz,<br>15-6L linear array Philips Sonos 7500 real-time 3D echoscannerB | 1 physical phantom<br>12 patients | No quantitative analysis of the *in vivo* results was performed. |
| Zahnd et al. (Zahnd, et al. 2015b) | 2015 | Local Phase-Based OF (Basarab, et al. 2009) | fr=91Hz<br>fs=50MHz,<br>fc=4MHz, fs50MHZ,<br>ULA-OP research scanner, | 20 young healthy volunteers<br>6 elderly patients | Longitudinal: 98±84 μm<br>Radial: 55±44 μm |
| Salles et al. (Salles, et al. 2015) | 2015 | Transverse oscillations (Liebgott, et al. 2010) | fr=10kHz<br>fc=5MHz<br>fs=40MHz<br>L14-5W/60 array Ultrasonix SonixTouch US system (Richmond, BC,<br>Canada) | - 3 artery numerical phantoms | Mean axial error: 4.2 ± 3.4 μm<br>Mean lateral errors:<br>9.9 ± 7.9 μm<br>the stiffnesses of the 3 vessel phantom walls investigated were estimated with an average relative error of 2.2%. |
| Hasegawa et al. (Hasegawa 2016) | 2016 | Phase tracking with frequency spectra | fr=1302Hz<br>fs=31.25 MHz<br>fc=7.5MHz<br>linear array PU-0558, Ueda Japan Radio) (scanner RSYS0002, Microsonic, Tokyo, Japan) | 1 phantom | Bias error 1D: Ra=11.5%, Lo=2.0%<br>Bias Error 2D: Ra= 3.0%, Lo= 2.0% |
| Zambacevičienė et al. (Zambacevičienė and Jurkonis 2019) | 2018 | Phase correlation and sub-sample algorithm | fr=52Hz<br>fs=40MHz<br>fc=14-5 MHz<br>Linear array<br>Scanner Ultrasonix sonixTouch (Analogic Ultrasound, Canada) | 1 phantom | NRMSE of detected motion amplitude: 0.21 to 0.41 μm and the coefficient of correlation-=<br>0.95 to 0.98 in case of any determined longitudinal motion function when the phase correlation, sub-pixel algorithm and additional filtering were used. |
| Miyajo et al. (Miyajo and Hasegawa 2018) | 2018 | Matching performed in the 2D Fourier domain | Scanner α-10, Aloka.<br>fr=3472Hz<br>fs=40MHz<br>fc=10MHz | 1 phantom<br>1 healthy volunteer | Bias error and standard deviation in the lateral velocity estimates: 0.048 and 0.282mm/s |
| Perrot et al. (Perrot, et al. 2018b) | 2018 | Video magnification | fr=2500Hz<br>fs=25MHz | 8 healthy volunteers | Motion magnification by a factor 1000 |

| | | | | | |
|---|---|---|---|---|---|
| | | | fc= 5MHz<br>Linear array (L7-4 )<br>(Scanner Verasonics Inc., Redmond, WA, USA)<br>Reconstruction technique: Stolts | | |

NRMSE= normalized root mean square error; fr=Frame rate, fs= Sample Frequency, fc=Center Frequency

Figure 1



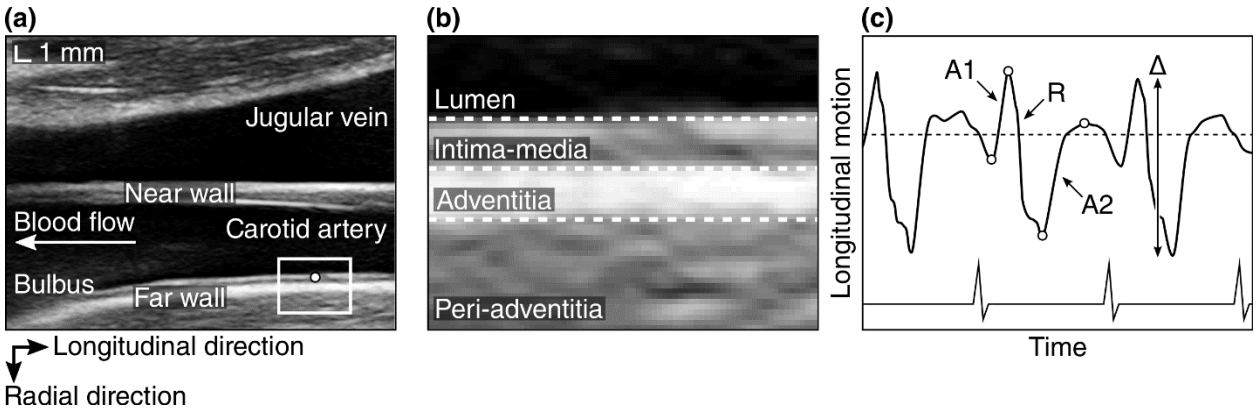

Figure 2a

Click here to access/download;Figure;Figure 2_a_Resubmitted.pdf

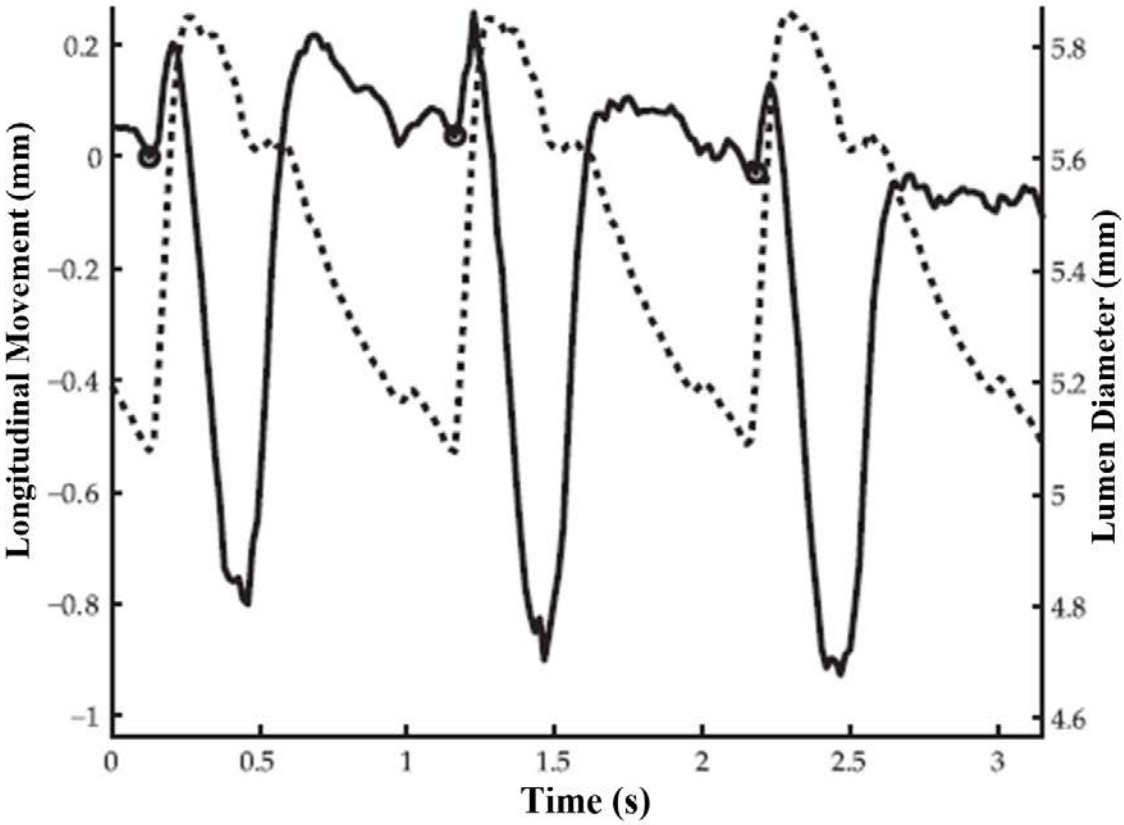

Figure 2b

Click here to access/download;Figure;Figure 2_b_Resubmitted.pdf

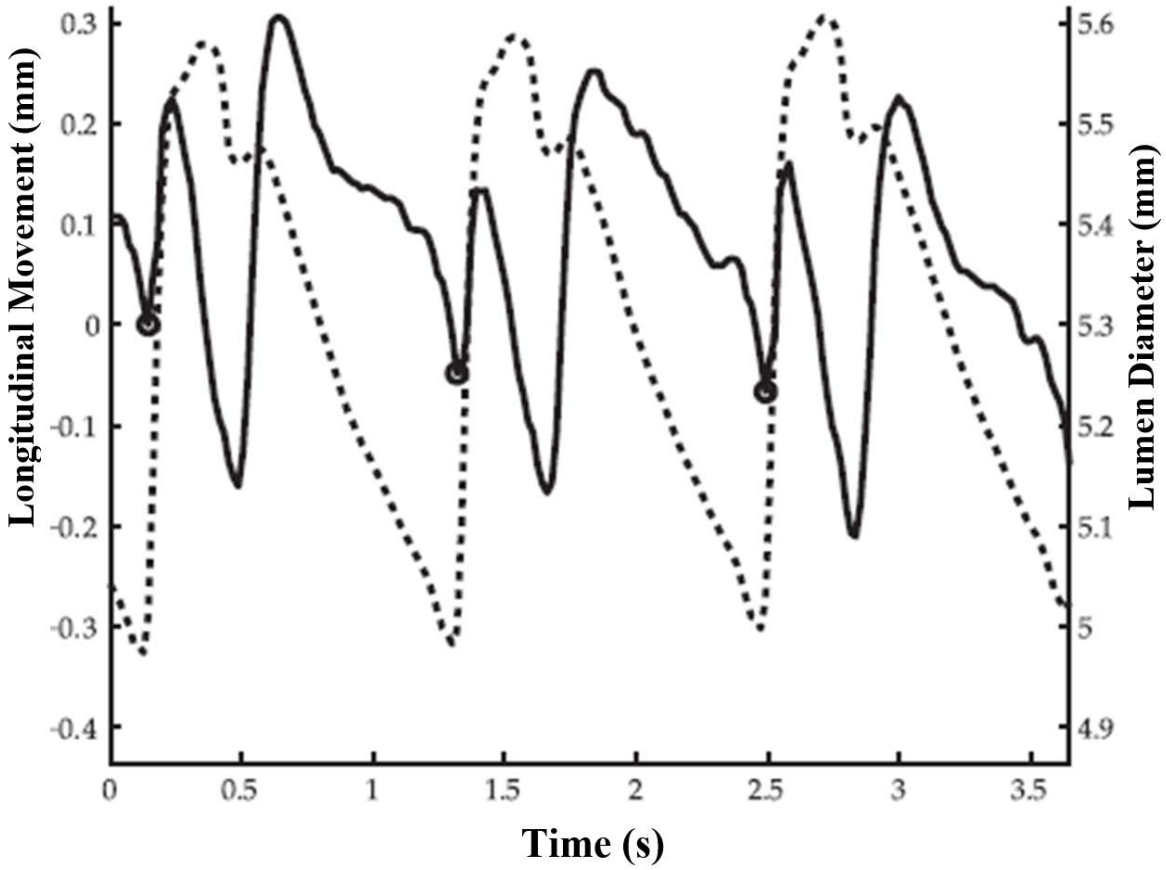

Figure 2c

Click here to access/download;Figure;Figure 2_c_Resubmitted.pdf

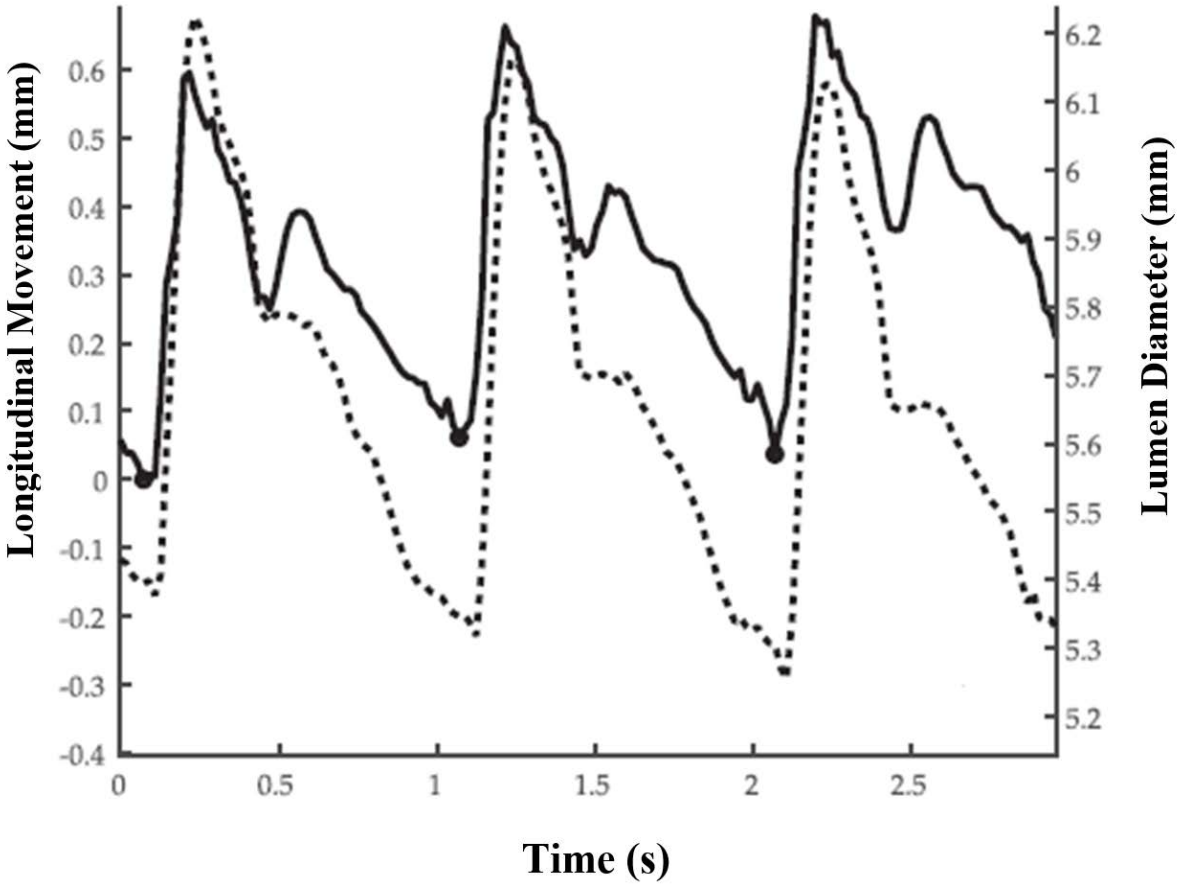

Figure 2d

Click here to access/download;Figure;Figure 2_d_Resubmitted.pdf

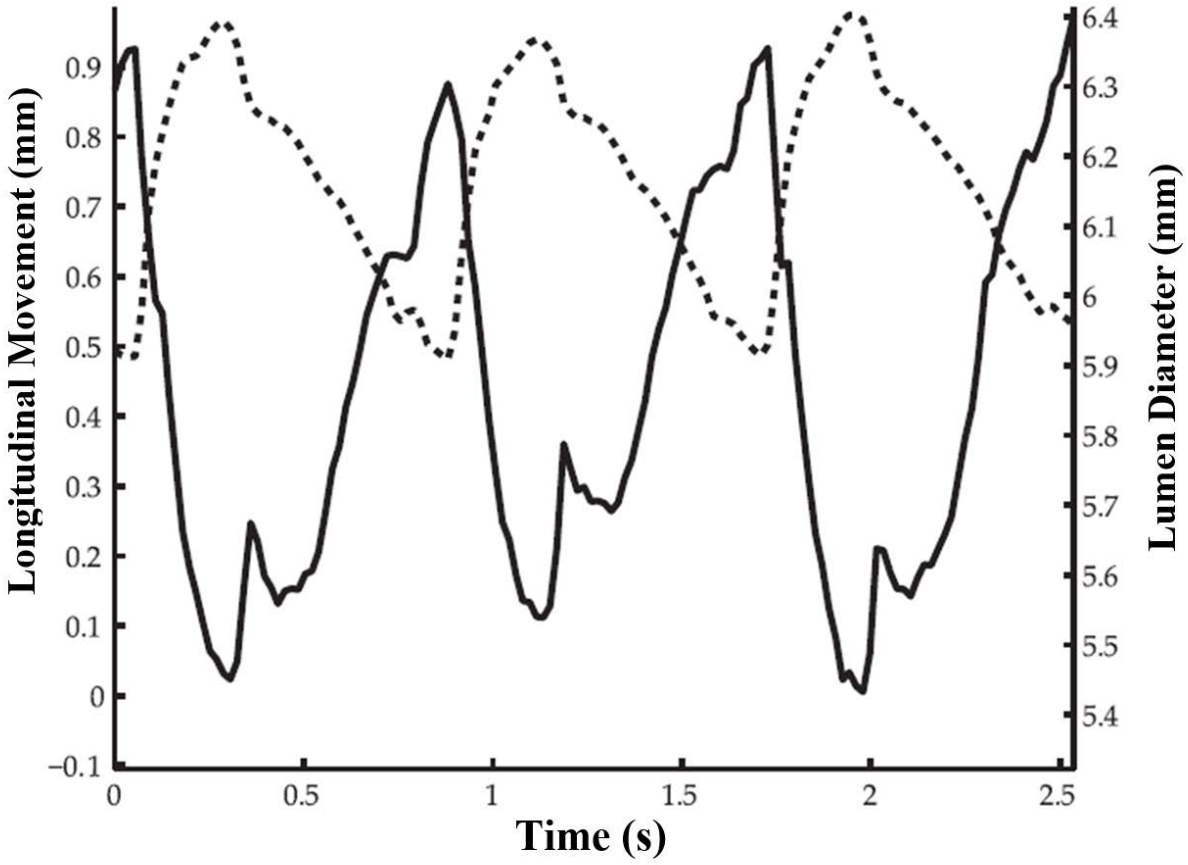

Figure 2e

Click here to access/download;Figure;Figure 2_e_Resubmitted.pdf

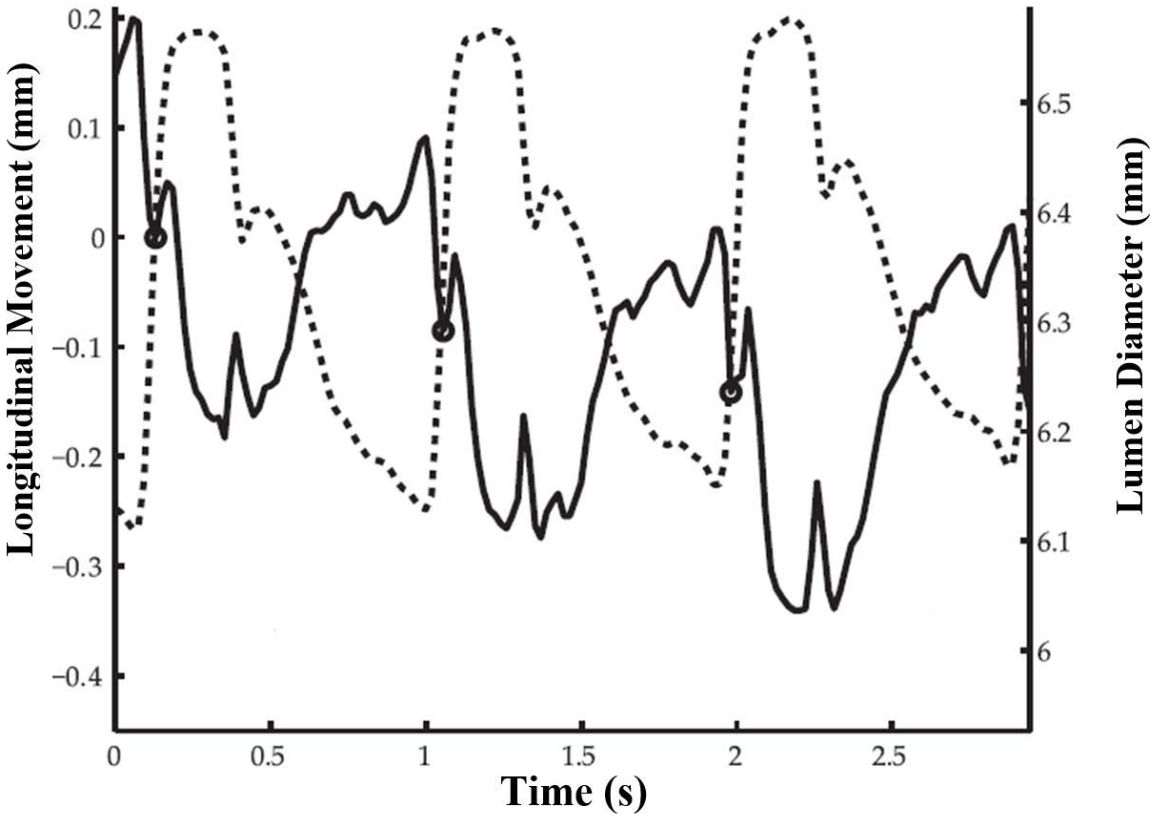

Figure 2f

Click here to access/download;Figure;Figure 2_f_Resubmitted.pdf

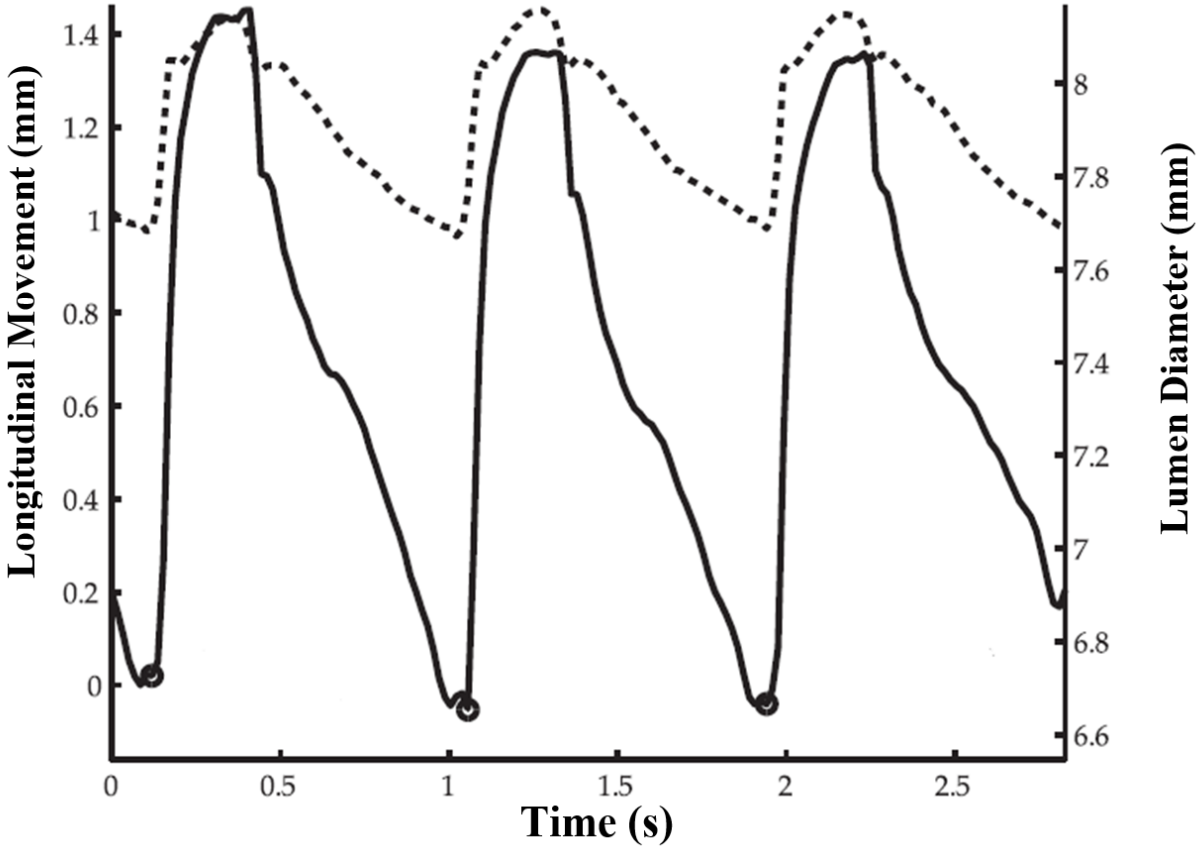

Figure 3a

Click here to access/download;Figure;Figure 3_a_Resubmitted.pdf

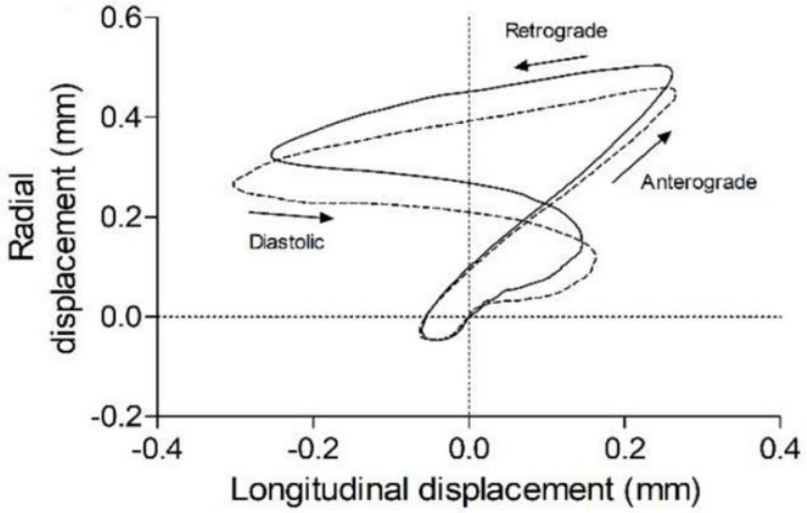

Figure 3b

Click here to access/download;Figure;Figure 3_b_Resubmitted.pdf